# The Evolution of Voids in the Adhesion Approximation

**Varun Sahni**[1], **B.S. Sathyaprakash**[1]

and

**Sergei F. Shandarin**[2]

[1] Inter-University Centre for Astronomy and Astrophysics
Post Bag 4, Ganeshkhind, Pune 411 007, India

[2] Department of Physics and Astronomy
University of Kansas, Lawrence, Kansas 66045, U.S.A.

**To appear in The Astrophysical Journal July 1994**

## ABSTRACT

We apply the adhesion approximation to study the formation and evolution of voids in the Universe. Our simulations – carried out using $128^3$ particles in a cubical box with side 128 Mpc – indicate that the void spectrum evolves with time and that the mean void size in the standard COBE-normalised Cold Dark Matter (hereafter CDM) model with $h_{50} = 1$, scales approximately as $\bar{D}(z) = \frac{\bar{D}_0}{\sqrt{1+z}}$, where $\bar{D}_0 \simeq 10.5$ Mpc. Interestingly, we find a strong correlation between the sizes of voids and the value of the primordial gravitational potential at void centers. This observation could in principle, pave the way towards reconstructing the form of the primordial potential from a knowledge of the observed void spectrum. Studying the void spectrum at different cosmological epochs, for spectra with a built in $k$-space cutoff we find that, the number of voids in a representative volume evolves with time. The mean number of voids first increases until a maximum value is reached (indicating that the formation of cellular structure is complete), and then begins to decrease as clumps and filaments merge leading to hierarchical clustering and the subsequent elimination of small voids. The cosmological epoch characterizing the completion of cellular structure occurs when the length scale going nonlinear approaches the mean distance between peaks of the gravitational potential. A central result of this paper is that voids can be populated by substructure such as mini-sheets and filaments, which run through voids. The number of such mini-pancakes which pass through a given void, can be measured by the *genus characteristic* of an individual void which is an indicator of the topology of a given void in initial (Lagrangian) space. Large voids have on an average a larger genus measure than smaller voids indicating more substructure within larger voids relative to smaller ones. We find that the topology of individual voids is strongly epoch dependent, with void topologies generally simplifying with time. This means that as voids grow older they become progressively more empty and have less substructure within them. We evaluate the genus measure both for individual voids as well as for the entire ensemble of voids predicted by the CDM model. As a result we find that the topology of voids when taken together with the void spectrum, is a very useful statistical indicator of the evolution of the structure of the Universe on large scales.

# I. INTRODUCTION

A remarkable feature of the large scale structure of the Universe is the presence of voids – volumes of order $10^3 h^{-3}$ Mpc$^3$, virtually devoid of the presence of galaxies. The existence of voids was spectacularly demonstrated with the discovery of the Bootes void an $\sim 10^5 h^{-3}$ Mpc$^3$ underdense region, by Kirshner et al. (1981). Since then successive redshift surveys (de Lapparant et al. 1986, Vogeley et al. 1991; Slezak et al. 1993), as well as deep pencil beam surveys (Broadhurst et al. 1990), have confirmed that voids are a salient feature of the large scale structure of the Universe, and that galaxies seem to lie preferentially along sheets and filaments separating voids.

Although it is generally agreed that voids account for most of the volume of the Universe, there is still considerable disagreement in the literature as to what is the typical size of a void. Part of this disagreement has to do with how one chooses to define voids. If voids are defined as underdense regions then the size of the void will obviously depend upon the density threshold below which an underdense region "becomes" a void. Clearly, the mean volume of underdense regions will always be larger than the mean volume of completely empty regions. The average size of a void in a sample will, in addition, be sensitive to the smallest voids which one recognizes. Clearly, if we recognize empty regions of diameter $\sim 0.2$ Mpc to be voids, then the mean void size will be much smaller than if we were dealing with voids having diameters $\geq 2$ Mpc.

However, even if we restrict ourselves to voids defined as completely empty regions, we still come across differing points of view as to the typical void size in the Universe. Thus, Kauffmann and Fairall (1991) (henceforth KF), who consider only void diameters larger than $\sim 5h^{-1}$ Mpc in an uncontrolled data sample, find from their catalogue of over 100 voids that the typical (*viz,* modal) size of a completely empty region is $D \sim 10h^{-1}$ Mpc. The mean void diameter in the KF sample is $36.5h^{-1}$ Mpc (Little 1992).[1] The authors also find no evidence of a cutoff in void size upto a maximum void diameter of 64 $h^{-1}$ Mpc. On the other hand, Vogeley et al. (1991), who work with a smaller but controlled sample (the CfA survey), find the maximum size of a completely empty region in their sample to be $\sim 20h^{-1}$ Mpc which is considerably smaller than the *mean void size* in the KF sample. A part of this discrepency may arise from the fact that KF work with a large but uncontrolled data sample, whereas the CfA survey although containing fewer galaxies has the advantage of being magnitude limited. (KF use galaxy redshifts which are not magnitude limited since they are compiled from many different sources, thereby giving rise to the "distinct possibility that certain regions of the sky are undersampled in comparison

[1] Little has evaluated the mean void diameter for 129 voids determined from the merged Southern Redshift Catalogue and the Catalogue of Radial Velocities of Galaxies and listed by KF in their paper.

to other regions " and to the related possibility that the existence of a particular void is due to undersampling rather than to any physical process (Kauffmann & Fairall 1991).) The other reason why the results of Vogeley et al. (1991) and those of KF differ, could be due to the different techniques used to actually measure void sizes. Thus, Vogeley et al. (1991) construct a void probability function for the CfA survey which measures the probability that a randomly selected volume in their survey contain no galaxies, whereas KF determine a void spectrum by filling regions empty of galaxies in their sample with cubes, the edge length of the largest cube filling a given empty region providing a measure of the void size. Although this method leads to a well defined algorithm to measure void sizes it suffers from the drawback (acknowledged by the authors) of ignoring the issue of void topology. (Voids in the KF sample are assumed a-priori, to possess a bubble like topology.)

Since voids are associated with positive peaks in the primordial gravitational potential, (Gurbatov, Saichev & Shandarin, 1985, 1989; Kofman & Shandarin, 1988) they give rise to anisotropies in the Cosmic Microwave Background Radiation (CMBR) via the Sachs-Wolfe effect: $(\delta T/T) \simeq \delta\phi/3$ on the surface of last scattering. This effect has been studied for individual voids by Blumenthal et al. (1992) who find the sizes of the largest voids to be smaller than $\sim 130h^{-1}$ Mpc (one void of this size within the horizon). In a later paper the same authors incorporate the COBE results to give a stronger limit $\sim 60h^{-1}$ to the maximal void size (Piran et al. 1993).

From the theoretical viewpoint the fact that voids might provide a key to understanding the large scale structure of the Universe was emphasised more than a decade ago, by Zeldovich & Shandarin (1982) and Zeldovich, Einasto & Shandarin (1982). Since then, the evolution of voids has been examined both analytically as well as numerically by a number of authors (Peebles 1982; Hausman, Olson & Roth 1983; Hoffman, Salpeter & Wasserman 1983; Fillmore & Goldreich 1984; Bertschinger 1985; Blaes, Villumsen & Goldreich 1990; Bonnor & Chamorro 1990; Regos & Geller 1991; Dubinski et al. 1992; van de Weygaert & van Kampen 1993; Harrington, Melott & Shandarin 1993). Semi-analytical spherically symmetric studies of voids have shown that large voids can often arise out of small initial negative density fluctuations. Numerical simulations by Bertschinger 1985 and Blaes, Villumsen & Goldreich 1990, confirmed that aspherical negative density perturbations grow to become more spherical with time (Icke, 1984) (the time-reverse of the Lin, Mestel & Shu (1965) instability), indicating that the evolution of negative density perturbations can often be treated as the time reversal of positive density ones. Since $|\delta\rho/\rho|$ never exceeds unity within a void, the linear approximation might be expected to hold for a longer period inside a void. Also, as voids tend to expand at faster rates than the mean Hubble flow of the Universe, matter within voids will have a tendency to to be swept up into two dimensional sheets separating neighboring voids. Both these considerations have led to the construction of a geometrical model of large scale structure based on Voronoi tesselation, in

which voids act as centers of repulsion and matter collects in sheets, filaments and nodes, which together make up the skeleton of the large scale structure of the Universe (Icke & van de Weygaert 1987; van de Weygaert 1991).

In this paper we propose to study the properties of voids using a semi-analytic approach to model non-linear gravitational instability, known as the adhesion approximation (Gurbatov, Saichev & Shandarin 1985, 1989; Shandarin & Zeldovich 1989). Since the adhesion model incorporates the Zeldovich approximation, we expect the predictions of the latter to be also valid for the former at early times. Most voids, according to the Zeldovich approximation, can be successfuly associated with peaks in the primordial gravitational potential. However, at late times, after shell crossing and the consequent breakdown of the Zeldovich approximation, the inherently nonlocal nature of the adhesion model begins to manifest itself. At such times, the location and size of a void is determined not so much by the location and height of peaks, as by the global structure of the primordial gravitational potential. As a result the association of peaks in the gravitational potential with voids, which exists in the Zeldovich approximation, begins to progressively breakdown at late times. The adhesion model, like the model based on Voronoi tesselation, describes the Universe in terms of a skeletal structure consisting of pancakes (sheets), filaments, clumps and voids. However, barring this resemblance, important differences exist between the two models. Namely, voids are not present *abinitio* in the adhesion model but arise out of dynamical considerations. Furthermore, the rich dynamical structure of the adhesion model allows it to address a number of important issues concerning voids, such as: Do voids evolve with time ? Are the voids seen today primary (i.e., first generation) or were they formed through the merger of an earlier generation of voids ? What is the likelyhood that voids will be populated by substructure such as mini-pancakes ? What is the topology of the large scale structure of the Universe ? *etc.* We shall attempt to address some of these questions plus a few more in the present paper.

The organisation of our paper is as follows:

We briefly discuss the adhesion approximation in section 2, and compare some of its predictions with those of the Zeldovich approximation, and N-body simulations. In section 3 we apply the adhesion model to obtain a distribution of void sizes – the void spectrum, for idealised primordial spectra $P(k) \propto k^n$, $n = -1, 0, +1$ (Melott & Shandarin 1993), as well as for more realistic initial conditions attempting to explain the large scale structure of the Universe, such as the cold dark matter model. We find that the void spectrum evolves with time – the mean void diameter increasing as the Universe expands. We also find that a distinct correlation exists between the mean void size and the value of the primordial gravitational potential at the void center – larger voids being associated with higher regions of the primordial potential. Our results also show that, in several instances a void can be multiply connected indicating a nontrivial topology, with minor pancakes (or filaments) running through a void that is circumscribed by major Zeldovich pancakes.

The void topology evolves with time, proceeding from a sponge like topology at early times, to a bubble like topology at late times. Our results concerning the void topology are summarised in Section 4. A discussion of our results is presented in section 5.

## II. THE ADHESION MODEL AND THE ZELDOVICH APPROXIMATION

The adhesion model is a logical extension of the Zeldovich approximation, which describes the evolution of density perturbations in a collisionless, self-gravitating medium, until the epoch of caustic formation and shell crossing (Zeldovich 1970; for review see Shandarin & Zeldovich 1989). We assume a spatially flat, matter dominated Universe: $\Omega_m = \Omega = 1, \Lambda = 0$.

Particle trajectories in the Zeldovich approximation, are described by the mapping

$$\vec{x}(\vec{q},t) = \vec{q} - a(t)\vec{\nabla}\Phi \tag{1}$$

where $\vec{q}$ is the initial (i.e., Lagrangian) comoving coordinate, and $\vec{x}$ is the final (i.e., Eulerian) comoving coordinate of a particle. $a(t)$ is the scale factor which coincides with the growing mode of the gravitational instability in a matter dominated spatially flat Universe. $\Phi$ is the linear velocity potential related to the primordial Newtonian gravitational potential $\phi$ by

$$\phi = A^{-1}\Phi \tag{2}$$

where $A = 2/(3H^2a^3)$, $H$ is the Hubble parameter: $H^2 \propto a^{-3}$ implying $A$ is a constant. The Poisson equation

$$\frac{\delta\rho}{\rho} = Aa(t)\nabla^2\phi \tag{3}$$

together with the linear growth law $\delta\rho/\rho \propto a(t)$, implies that the linearised Newtonian potential $\phi$, like its counterpart the velocity potential $\Phi$, does not depend upon time.

The continuity equation $\rho(x)d^3x = \rho(q)d^3q$ ($\rho(x)$ is the Eulerian density, and $\rho(q) = \bar{\rho} = constant$ is the Lagrangian density), when combined with the Zeldovich approximation (1) describes the deformation of an infinitesimal volume element in terms of the Jacobian of the transformation from $\vec{q}$ to $\vec{x}$, so that

$$\frac{dV_E}{dV_L} = J\left[\frac{\partial\vec{x}}{\partial\vec{q}}\right] = \left|\delta_{ij} - a(t)\frac{\partial^2\Phi}{\partial q_i \partial q_j}\right| \tag{4a}$$

and, as a result

$$dV_E = dV_L\,[1 - a(t)\lambda_1(q)]\,[1 - a(t)\lambda_2(q)]\,[1 - a(t)\lambda_3(q)] \tag{4b}$$

where $dV_E$ and $dV_L$, are the volume elements in Eulerian space (E-space) and Lagrangian space (L-space) respectively, and $\lambda_1, \lambda_2$ and $\lambda_3$ are the eigenvalues of the deformation tensor $\psi_{ij}$ :

$$\psi_{ij} \equiv \frac{\partial^2 \Phi}{\partial q_i \partial q_k}.$$

From (4b) we see that one (or more) of the eigenvalues $\lambda_i$ have to be positive, in order for (4) to describe a contraction along one (or more) axis (*i.e.*, $dV_E < dV_L$). On the other hand all three eigenvalues $\lambda_1, \lambda_2, \lambda_3$ must be negative, in order for the volume element to expand along all three axis (*i.e.*, $dV_E > dV_L$). It is well known that in the Zeldovich approximation, the condition ($dV_E < dV_L$), ultimately gives rise to the formation of caustics such as pancakes, filaments and clumps, whereas the opposite condition ($dV_E > dV_L$) determines voids. The validity of (4) breaks down soon after the formation of caustics, which occur when $a(t) = min\{1/\lambda_i\}$. Thereafter the thickness of pancakes grows unbounded in the Zeldovich approximation, which runs counter to the findings of N-body simulations which show that the thickness of pancakes remains considerably smaller than both the pancake size as well as the mean distance between pancakes. In order to stabilise the thickness of pancakes, a mock viscosity term, which mimicks the effects of nonlinear gravity, must be incorporated into the Zeldovich approximation.

To see how this may be done, consider the Euler equation

$$\frac{\partial \vec{v}}{\partial t} + \frac{1}{a}(\vec{v}\ \nabla)\vec{v} + H\vec{v} = -\frac{1}{a}\nabla\phi \tag{5}$$

where

$$\vec{v} = a\frac{d\vec{x}}{dt},$$

$\vec{x}$ being the comoving coordinate of the particle (or fluid element). In terms of the new comoving velocity variable

$$\vec{u} = \frac{d\vec{x}}{da} = \frac{\vec{v}}{a\dot{a}},$$

(5) can be recast as (Kofman 1991)

$$\frac{\partial \vec{u}}{\partial a} + (\vec{u}\ \nabla)\vec{u} = -\frac{3}{2a}(\vec{u} + A\nabla\phi) \tag{6}$$

The right hand side of equation (6) is reminiscent of a force term, in the Lagrangian approach. Setting it to zero we obtain the Zeldovich approximation. In the adhesion approximation, we replace the right hand side of equation (6) by a viscosity term which mimicks the adhesive effects of nonlinear gravity. As a result the Euler equation for the velocity field becomes

$$\frac{\partial \vec{u}}{\partial a} + (\vec{u}\ \nabla)\vec{u} = \nu\ \nabla^2\vec{u} \tag{7}$$

which is the Burgers equation (Burgers 1974). For potential flows equation (7) has the following exact analytical solution

$$\vec{u}(\vec{x},a) = \frac{\int d^3q \ \frac{(\vec{x}-\vec{q})}{a(t)} \ \exp\left(\frac{1}{2\nu}G(\vec{q},\vec{x},a)\right)}{\int d^3q \ \exp\left(\frac{1}{2\nu}G(\vec{q},\vec{x},a)\right)} \tag{8}$$

where

$$G(\vec{q},\vec{x},a) = \Phi(\vec{q}) - \frac{(\vec{x}-\vec{q})^2}{2a(t)},$$

$\Phi(\vec{q})$ is the potential of the linear velocity field introduced earlier: $\vec{u}(\vec{x},a=0) = -\vec{\nabla}\Phi$. For small values of the viscosity parameter $\nu \rightarrow 0$, the integrals in equation (8) can be evaluated using the method of steepest descents. This leads to the following condition being imposed on the gradient of the gravitational potential:

$$\nabla_{\vec{q}} P(\vec{q};\vec{x},a) = \nabla_{\vec{q}}\Phi(\vec{q}) = A\nabla_{\vec{q}}\phi(\vec{q}) \tag{9}$$

where

$$P(\vec{q};\vec{x},a) = \frac{(\vec{x}-\vec{q})^2}{2a(t)} + P_0.$$

Equation (9) has an elegant geometrical interpretation which can be summarised as follows: Whether or not a particle originally located at $q_0$ is stuck within a pancake can be found by descending a paraboloid $P(q;x,a)$ with radius of curvature $2a(t)$ and height $P_0$ onto the linear gravitational potential $\phi$, in such a manner so as to be tangential to the potential at $q_0$ (see Fig. 1). (The height of the paraboloid $P_0$ is a free parameter uniquely determined by the condition that $P(\vec{q},\vec{x},t)$ osculates $\phi(\vec{q})$ at $q_0$. We use $\phi$ and $\Phi$ interchangeably, since $\phi \propto \Phi$ if the Universe is flat and matter dominated). If the paraboloid so constructed touches or intersects the potential at any other point $q \neq q_0$, then we say that the particle in question has already entered a caustic (Fig. 1, middle and bottom panels), otherwise it has not (Fig.1, top panel). Thus, one can divide the Lagrangian space at any given time into *stuck* and *free* regions. Stuck regions correspond to particles already in caustics, whereas free regions are still expanding via the Zeldovich relations (1,4) and correspond to voids. The apex of the paraboloid $\vec{x}$, which osculates the potential in two or more points (without intersecting elsewhere) describes the location of the caustic in Eulerian space. The mass in caustics (clumps) in Fig. 1 is given by $m_1 = |q_1 - q_2|\ \bar{\rho}$, $m_2 = |q_3 - q_4|\ \bar{\rho}$, and $M = |q_1' - q_4'|\ \bar{\rho}$, $\bar{\rho}$ being the mean density. (The clumps are drawn so that the clump radius is proportional to its mass.) The velocities of the caustics can be found from $\vec{u} = d\vec{x}/da = (\phi_{q_i} - \phi_{q_j})/(q_i - q_j) \times \vec{n}$, where the unit normal $\vec{n}$ points from a higher value of the gravitational potential towards a lower value. (For earlier implementations of the adhesion model using the geometric approach, see Kofman, Pogosyan & Shandarin 1990, Sahni 1991, Williams et al. 1991, Kofman et al. 1992. For an alternative implementation of the adhesion approximation see Nusser & Dekel 1990, and Weinberg & Gunn 1990.)

The skeleton of the large scale structure can be derived from the division of *L-space* into stuck and free regions, by noting that the border between these regions consists of particles which are only *just* entering into caustics. Since the Zeldovich approximation is valid right until a particle ends up in a caustic, we can determine the precise location of caustics in *E-space* by moving the border between stuck and free Lagrangian regions by means of the Zeldovich approximation. We do this for different values of $\sigma(t)$ defined in units of the *rms* linear density contrast on the grid scale:

$$\sigma(t) = \left\langle (\delta\rho/\rho)^2 \right\rangle^{\frac{1}{2}} \equiv \left[ a^2 \int_0^\infty P(k) k^{N_D - 1} dk \right]^{\frac{1}{2}}, \tag{10}$$

where $N_D$ is the dimensionality of the space. Our results are shown in Fig. 2 a-e. In Fig. 2a, b the distribution of caustics (dots) was obtained by moving the border between stuck (unshaded) and free (shaded) Lagrangian regions by means of the Zeldovich approximation (equation (1)). The area of clumps in Fig. 2c is drawn proportional to the clump mass obtained using the adhesion approximation. Comparison of the adhesion model (Fig. 2b), with the two-dimensional N-body simulations of Melott and Shandarin 1989 (Fig. 2d), shows very good agreement at an epoch when the Zeldovich approximation (Fig. 2e) breaks down.

An interesting question concerns the percolation of *stuck* and *free* regions in L-space. From Fig. 2 a-c we clearly see that for small values of $\sigma$ ($\sigma < \sigma_1$) the free phase percolates (Fig. 2a), whereas for large values of $\sigma$, ($\sigma > \sigma_2$), percolation occurs in the *stuck* phase (Fig. 2c). It would be interesting to estimate the values of $\sigma_1, \sigma_2$, and their dependence on the power spectrum $P(k)$. It would also be interesting to determine whether an epoch exists, when both phases percolate (i.e., whether $\sigma_2 < \sigma_1$). These questions might shed some light on the issue of the large scale topology of the Universe (i.e., whether "bubble-like" or "sponge-like"), and will be examined in detail in a forthcoming paper (Sahni, Sathyaprakash & Shandarin 1993).

The geometrical picture of the adhesion model, allows us to make some general statements regarding the relative concentration of matter in clumps, filaments, pancakes and voids, which are the structural units constituting the skeleton of the large scale structure of the Universe in three dimensions. The whole process of structure formation can be viewed as a mapping of the space at the initial time when the density is virtually homogeneous (the Lagrangian space) into the space at the time in question (the Eulerian space). All structural units except voids have at least one dimension $\varepsilon$ (thickness) which is much smaller than the other dimensions $\varepsilon \ll L$ . $\varepsilon$ is determined by the relaxation processes and in the adhesion model is parametrised by the viscosity coefficient $\nu$. The limiting case $\nu \to 0$ is accompanied by $\varepsilon \to 0$ (for the relation between $\varepsilon$ and $\nu$ see Gurbatov, Saichev & Shandarin 1989) and, as a result, clumps become points, pancakes become sheets of infinitesimal thickness etc. In this case, at late times, the mapping becomes formally

degenerate: clumps correspond to the mapping of three-dimensional volumes onto zero-dimensional points ($3D \rightarrow 0D$), filaments correspond to the mapping of two-dimensional surfaces onto one dimensional lines ($2D \rightarrow 1D$), pancakes correspond to the mapping of one-dimensional lines onto two-dimensional surfaces ($1D \rightarrow 2D$), and voids ($0D \rightarrow 3D$).

The relative concentration of matter within these structural units can be qualitatively characterized by two numbers $\mathcal{D}_L, \mathcal{D}_E$, specifying the type of mapping $\mathcal{D}_L \rightarrow \mathcal{D}_E$ : $\mathcal{D}_E$ is the dimension of the object in E-space, which is formed from matter originally spread uniformly in a $\mathcal{D}_L$ dimensional volume in L-space. Of course, the mapping of a higher dimensionsional set onto a lower dimensional set (clumps and filaments) formally results in infinite density, however of different types. Clumps, corresponding to the $3D \rightarrow 0D$ mapping are much higher concentrations of mass than filaments which result from the $2D \rightarrow 1D$ mapping. In addition, filaments originating from a $2D$ set in $3D$ space have infinitesimal mass which means that they eventually vanish in real systems. Voids and pancakes result from the $0D \rightarrow 3D$ and $1D \rightarrow 2D$ mappings respectively and therefore tend to have both infinitesimal densities and masses at later times.

This discussion may be useful in providing a guideline for a qualitative understanding of the evolution of the structural units with time as well as for comparing $3D$ and $2D$ systems. In two-dimensional space clumps correspond to the $2D \rightarrow 0D$ mapping, filaments to the $1D \rightarrow 1D$ mapping and voids to the $0D \rightarrow 2D$ mapping. Therefore one may expect filaments in two-dimensional simulations ($1D \rightarrow 1D$) to appear relatively more conspicuous when compared to pancakes ($1D \rightarrow 2D$) in three-dimensional simulations. On the other hand filaments in three-dimensional simulations ($2D \rightarrow 1D$) must look more noticeable than their counterparts in two dimensions. We believe that this type of reasoning is worth keeping in mind when extrapolating (even qualitatively) conclusions from $2D$ to $3D$.

## III. THE VOID SPECTRUM AND ITS EVOLUTION

It is worth contrasting the dynamical picture of voids which emerges in the adhesion model, with the essentially static picture that follows from the Zeldovich approximation. In the Zeldovich approximation, voids are associated with Lagrangian regions in which all the eigenvalues of the deformation tensor are negative. This implies essentially, that there is a one to one correspondence between voids and peaks in the primordial gravitational potential. This is also true at early times in the adhesion model when the paraboloid is very narrow and can only feel small localised regions of $\phi$ (see Fig. 1, top panel). The adhesion model at such times gives essentially the same results as the Zeldovich approximation. At late times however, the radius of curvature of the paraboloid can become comparable to that of the initial gravitational potential, with the result that the paraboloid is now able to *survey* larger regions of the potential. It is at this stage that the essentially nonlocal nature of the adhesion model emerges. As a result, a free region in L-space (a void) can

become *stuck* at late times, even if it lies in the vicinity of a peak in the gravitational potential (see Fig. 1, bottom panel). As a result, no strictly one to one relationship exists between voids and peaks in the gravitational potential, in the adhesion model. In addition, voids in L-space tend to shrink in the adhesion approximation, whereas in the Zeldovich approximation, their volume in L-space remains constant. (By contrast the total volume of voids in E-space remains constant in the adhesion model.) The distinction between voids in the Zeldovich approximation and in the adhesion model in two-dimensions, is brought out clearly in Fig. 3 in which we superimpose voids in the Zeldovich approximation with those obtained using the adhesion model. From Fig. 3 we see that virtually all of the voids in the adhesion model, constitute a subclass of voids in the Zeldovich approximation, although this is strictly true only at very late times, when most of the matter is already in pancakes, so that the volume (equivalently, area in 2D) occupied by voids in L-space, is very small. The terms *early* and *late* can be quantified in relation to the *rms* linear density contrast on the grid scale $\sigma(t)$ defined in equation (10), which evolves in proportion to the expansion factor of the Universe. (The adhesion picture plotted in Fig. 3, corresponds to $\sigma = 8$.)

The geometrical ansatz which allows us to divide L-space into stuck and free regions, also provides us with a very elegant way to determine both the individual void size, as well as the entire void spectrum. As discussed in the previous paragraph, a void in L-space is a region, matter from which has not yet fallen into a caustic. Since the Zeldovich approximation is still valid in such regions, one can use the volume deformation formula given by equation (4b), to determine the Euler volume occupied by a unit cubical element in L-space. Summing over all such elementary volume elements within a given Lagrangian void gives the volume of the void in E-space:

$$V_E = \sum dV_E = \sum_{i=1}^{N} dV_L \; [1 - a(t)\lambda_1(q_i)]\,[1 - a(t)\lambda_2(q_i)]\,[1 - a(t)\lambda_3(q_i)] \qquad (11)$$

where $N$ denotes the number of elementary *free* volume elements in a given L-space void.

(Note that voids in L-space are defined on a discrete grid, whereas those in E-space are *not*. Consequently $V_L = N dV_L = N(\lambda_N/2)^3$ gives the volume of the void in L-space, where $\lambda_N$ is the Nyquist wavelength.)

This method, which is a useful synthesis of both the adhesion as well as the Zeldovich approximations, allows us to determine the precise volume of a void without resorting to any simplifying assumptions regarding its shape, such as sphericity, *etc.*, though it neglects the volume occupied by clumps, filaments and pancakes. We apply this ansatz to determine the spectrum of void sizes, for a Cold Dark Matter model with $\Omega = 1$, $H_0 = 50$ km/sec/Mpc, and amplitude normalised by the COBE observed CMBR anisotropy (The COBE - normalised amplitude gives $(\Delta M/M) \simeq 1.1$ for the *r.m.s.* CDM mass

fluctuation on scales of $8h^{-1}$ Mpc (Smoot et al. 1992, Efstathiou, Bond & White 1992). The corresponding value of $\sigma(t)$ is 9.)[2].

The results of our simulations, which average three realisations of the CDM spectrum using $128^3$ particles, in a 128 Mpc box with periodic boundary conditions, are shown in Fig. 4 for different cosmic epochs corresponding to: (a) the past $a = 0.5\ a_0$, $z = 1$ (top panel); (b) the present $a = a_0$, $z = 0$ (middle panel); and (c) the future (!) $a = 1.5\ a_0$ (bottom panel); ($a$ – is the expansion factor, and $z$ the redshift). We plot both the number fraction of voids (right panels) having a given diameter: $n(D)/N$, $N = \sum_i n(D_i)$, as well as the associated void volume fraction (left panels): $v(D)/V = n(D) \times V_E(D)/V$, $V = \sum_i V_E(D_i)$. (The void diameter in our simulations is defined so that $4\pi(D/2)^3/3 = V_E(D)$, where $V_E$ is the void volume in Eulerian space, described by equation (11).) The void spectrum in the middle panel of Fig. 4 has been plotted for $\sim 3400$ voids, – the mean number of voids at the present epoch in our simulation. We find that the volume spectrum of voids shows a fairly uniform spread for voids having diameters in the range $10 \leq D \leq 30$ Mpc where $D$ is the void diameter. Approximately 65% of the total volume in voids, is contained in voids lying within this range. By contrast, the number spectrum of void sizes, has a well defined peak on scales of $\sim 6$ Mpc, indicating that the most abundant voids in our simulation ($\sim 50\%$) are of this size. However, the net contribution from such small size voids, to the overall void volume is a tiny $\sim 10\%$.

From Fig. 4 we see a distinct evolution of the void spectrum with cosmological epoch, the average size of a void growing roughly with time as $\bar{D}(z) = \bar{D}_0/\sqrt{1+z}$, where $\bar{D}_0 \simeq 10.5$ Mpc, is the mean diameter of a void today and $z$ is the cosmological redshift. [3] (The modal diameter of a void in our simulations turns out be slightly larger: $D_{mode} \simeq 17$ Mpc. The maximum void size in our simulations is $\simeq 60$ Mpc.)

The void spectrum obtained by us using the adhesion model, may be compared with the void spectrum reconstructed by KF from a preliminary catalogue of 129 voids . (The voids in our simulations are empty regions, the density of matter in a void being less than 1% of the mean density of matter in the Universe. Likewise the voids in the KF sample are also assumed to be empty.)

---

[2] In normalising the CDM spectrum, we have ignored the gravity wave contribution to $(\Delta T/T)$, which in some cases can be significant (Davis et al. 1992, Liddle &Lyth 1992, Lidsey & Coles 1992, Lucchin et al. 1992, Sahni & Souradeep 1992, Salopek 1992, Souradeep & Sahni 1992).

[3] The mean void diameter is evaluated using $4\pi(\bar{D}/2)^3/3 = \bar{V}$, where $\bar{V} = N^{-1}\sum_{i=1}^{N} V_i$ is the mean void volume. Taking an alternate definition for $\bar{D}$ : $\bar{D} = N^{-1}\sum_{i=1}^{N} D_i$ results in a somewhat smaller value $\bar{D} \simeq 7$ Mpc.

KF obtain $D_{mode} \simeq 8 - 11h^{-1}$ Mpc, $h = H/100$, for the typical (viz modal) diameter of a void in their catalogue. Applying the same criteria as KF, and considering only voids having diameters greater than $5h^{-1}$ Mpc in our sample, we find the mean, median and modal void sizes in our simulations to be $D_{mean} = 19.1 \pm 0.3$ Mpc, $D_{median} = 26.4 \pm 0.8$ Mpc, and $D_{mode} = 25 \pm 5$ Mpc respectively, at the present epoch.[4] As a result we find that the modal diameter of a void in our sample is just about the same as that in the KF sample. (However, the mean diameter of a void in our simulations appears to be smaller than that implied in the KF survey.) The good agreement shown between the observed modal void size and that predicted by the CDM model must however be treated with some caution, since (a) the modal void size in our CDM simulations is subject to fairly large uncertainties (in fact, we do not have a well defined modal value at all) and (b) the methods we employ to determine the void size and those employed by KF are somewhat different. Namely, KF work with an uncontrolled data set and may therefore be systematically overestimating void sizes. KF further make the assumption that voids are essentially compact so that two neighboring voids do not percolate, they then determine the void size by inscribing the given void with a cube – the edge length of the cube providing a measure of the void size. While this method has the advantage of providing a well defined implementational algorithm to determine void sizes, it suffers from the drawbacks that: (i) voids are assumed to be approximately ellipsoidal with comparable axes, and (ii) because voids are assumed to be isolated, the possible sponge-like topology of voids is ignored. Neither of these assumptions is made in the adhesion model, in which the void volume is calculated for voids which can have virtually any shape and topology – a point that we shall elaborate on in the next section. Consequently, in order to rule out (or confirm) the predictions made by the CDM model, we must apply the same void finding algorithm both to the data as well as to the simulations. We propose to do this in a follow up paper.

An important related issue which we have been unable to adequately settle in the present paper concerns the distribution of void sizes in a realistic (i.e., spatially unbounded) CDM Universe. Simulations performed by us on $64^3$ Mpc$^3$ and $128^3$ Mpc$^3$ sample volumes of a CDM Universe show that, although larger voids are present in the $128^3$ sample relative to the $64^3$ one, the mean void size does not change much. We get a value of $D_{mean} \simeq 10$ Mpc (18 Mpc) in a $64^3$ sample and $D_{mean} \simeq 10.5$ Mpc (19 Mpc) in a $128^3$ sample. (The numbers quoted in parentheses are those obtained after discarding all voids of size less than 10 Mpc as in KF.) This could indicate that the mean diameter of voids converges rapidly in an $\Omega = 1$ CDM Universe so that the results which we quote for $D_{mean}$ from our $128^3$

[4] The mean, median and mode are defined with respect to the void volume fraction. Voids having the modal void size therefore provide the largest contribution to the overall void volume spectrum. Evaluating statistical averages for the void number spectrum, gives much smaller values both for the median as well as the modal void size due to the abundance of small voids in the CDM simulation.

simulations could be representative of the entire CDM Universe. However, this issue can be completely resolved only after larger simulations have been performed. (Incidentally, the maximum void size increases from $D_{\max} \simeq 40 \pm 8$ Mpc in a $64^3$ simulation to $D_{\max} \simeq 57 \pm 6$ Mpc in a $128^3$ simulation.) We would also like to mention in this connection, that the median (evaluated with respect to the void number spectrum) is usually a considerably more stable statistical indicator of void sizes than the mean. The reason for this is that the median is much less sensitive to the presence of a few very large voids in a sample than the mean, and consequently its value does not grow as rapidly as the latter as we increase the sample size of our model Universe. (See also Kauffmann & Melott 1992).

Fig. 1 shows that one might expect to see a correlation between the sizes of voids, and the height of the linear gravitational potential, especially at late times. This feeling is borne out by the results of our simulations for the CDM model (see Fig. 5), which show that a distinct correlation exists between the size of a void, and the value of the gravitational potential evaluated at its center. The value of the potential averaged over all the void centers at the present epoch is about 0.75 times the *rms* value of the potential, indicating that voids preferentially form in those regions where the gravitational potential is large. In order to demonstrate the general nature of this relationship between void size and the value of the gravitational potential $\phi$, we have also analyzed simulations for power law primordial spectra: $P(k) = \langle |\delta_k|^2 \rangle \propto k^n$, where $|\delta_k|$ is the spatial Fourier transform of the density contrast (see Melott & Shandarin 1993). It is assumed that the phases of the Fourier components are randomly distributed, so that the gravitational potential $\phi(x)$ has the statistical properties of a Gaussian random field. A cutoff was introduced into the spectrum by requiring that $P(k) = 0$ for $k > k_c$. (Physical processes which can give rise to such a cutoff include the free streaming of weakly interacting massive particles (WIMP's) such as massive neutrino's, and the Silk damping of inhomogeneities in the photon-baryon plasma.) Our simulations were run on a $128^3$ box for the following three models: $n = -1, 0, +1$, and $k_c = 16 \times k_f$. ($k_f$ is the wavenumber of the fundamental mode: $k_f = 2\pi/L$ where $L$ is the length of the side of the simulation cube.) Three simulations were performed for each of the three spectra amounting to 9 simulations in all.

Our results are shown in Fig. 6 for different values of $\sigma(t)$. The upper limit in the integral in equation (10) is effectively replaced by $k_N$ – the Nyquist frequency in the simulation. $\sigma(t)$ can be related to $k_{NL}$ – the wavenumber of a mode going nonlinear at the given epoch:

$$\left\langle (\delta\rho/\rho)^2 \right\rangle \equiv \frac{a^2}{2\pi^2} \int_0^{k_{NL}} P(k) k^2 dk = 1 \tag{12}$$

so that

$$\sigma(t) = \left( \frac{\int_0^{k_N} P(k) k^2 dk}{\int_0^{k_{NL}} P(k) k^2 dk} \right)^{1/2} . \tag{13}$$

We see that for truncated power law spectra ($n > -3$)

$$\sigma(t) = \left(\frac{k_c}{k_{NL}}\right)^{\frac{n+3}{2}}, \tag{14}$$

consequently, $k_{NL}$ decreases with epoch, as successively larger scales enter the nonlinear regime. We do not evolve our simulations beyond the epoch when the largest scale to go nonlinear equals the box size.

From Fig. 6 we find that as in the case of the CDM model, a marked correlation exists between the diameter of a void and the value of the gravitational potential at its centre at late times. We also find that the mean value of the potential evaluated at void centers

$$\langle\phi\rangle = \frac{1}{N}\sum_{i=1}^{N}\phi_i,$$

$N$ being the number of voids in a simulation, increases with time, being larger at a given instant of time, for steeper spectra (see Fig. 7). $\langle\phi\rangle/\phi_{rms} \propto \sqrt{\sigma(t)}$ provides a reasonably good approximation, especially at late times, to the rate of growth of $\langle\phi\rangle$ for the power law spectra considered by us.

¿From figures 5, 6 we find that the correlation between diameter and potential is more striking for spectra with more short range power (such as the truncated $n = 1$ spectrum). This may be because a potential having significant long range power (such as CDM) has features on it (small scale *wiggles* superimposed on long range *mountains* and *valleys*) which will influence the sites of void formation. As a result a small wiggle in the potential will generally give rise to a small void even if the wiggle occurred at a large value of $\langle\phi\rangle/\phi_{rms}$. (The dip in $\langle\phi\rangle/\phi_{rms}$ occuring for void dimaters $10 - 20$ Mpc. in figures 5, 6, which is more pronounced for spectra with more large scale power, is a distinctive feature of this effect.) This modulation in the void spectrum caused by low frequency waves in the potential, will lead to a more noisy relation between the void diamter and $\langle\phi\rangle/\phi_{rms}$ for spectra with significant large scale power, as is indeed demonstrated in figures 5,6.

The correlation of void sizes with the "height" of the gravitational potential seen in Fig. 5 and 6, raises the interesting possibility of reconstructing the primordial form of $\phi$ from the observed form of the void spectrum. The primordial form of the gravitational potential is determined both by physical processes occuring in the very early Universe (such as Inflation), as well as by the nature of dark matter, hence some indications as to its form would be of immense value (see also Kofman & Shandarin 1988).

The evolution of the void spectrum and the transfer of power from smaller to larger voids at late times which was shown to occur for the CDM model is demonstrated with great clarity in Fig. 8 for power law spectra. (Note particularly the evolution of the void

number histogram shown in Fig. 8 b-d and the corresponding evolution of the mean and maximum void sizes in Fig. 9a.) We find that for large voids $V > V_{mean}$ the number spectrum of voids in Fig. 8b - 8d is well fitted by the exponentially decaying function $\exp(-V/V_*)$ where $V_* \propto V_{mean}$ . A similar result was also obtained by Kofman et al. (1992) for the two dimensional case.

From Fig. 9a we find that the mean void diameter grows very nearly as $D_{mean} \propto \sqrt{a(t)}$ at late times. (The complementary picture demonstrating the evolution of the total number of voids in our simulations is shown in Fig. 9b.) For the truncated scale invariant spectrum $n = 1$, this result agrees with an asymptotic analysis of the growth of cellular structure in the adhesion model made by Gurbatov et al. (1985, 1989), who found that $D_{mean} \propto \sqrt{a(t)}$ if $n \geq 1$, and $D_{mean} \propto a(t)^{2/(n+N_D)}$ ($N_D$ being the dimensionality of space) for $-1 < n < 1$. The last result suggests that the mean void size grows faster for spectra with more large scale power, and is seemingly at odds with our analysis which indicates that $D_{mean} \propto \sqrt{a(t)}$ for $-1 \leq n \leq 1$. This discrepency might arise because of the following two reasons: a) In their analysis Gurbatov et al. implicitly assume that voids are associated with peaks in the gravitational potential. We find on the other hand, that this assumption is not always satisfied, since voids can sometimes be associated with other features in the potential such as ridges etc. (this is especially true in two and three dimensions.) As a result the analysis of Gurbatov et al. is strictly valid at asymptotically late times. b) Our simulations are carried out in a finite sized box which might inhibit the late time growth of voids particularly for fluctuation spectra with long range power. A similar effect was earlier discussed by Kofman et al. (1992) in the context of the two dimensional adhesion model. Indeed, simulations conducted by us on spectra having no small scale cutoff show that $D_{mean}$ grows proportionally to $a(t)^{2/(n+N_D)}$ for $n = 0, -1$ as expected.

An interesting feature which emerges from our simulations with a cutoff in the initial spectrum is that the number of voids peaks at a given value of the expansion factor $\sigma(t) = \sigma_*$, and then declines steadily (see Fig. 9b). The value of $\sigma_*$ is relatively insensitive to the form of the spectrum for spectra with $k_c \gg k_f$, and can be described by the analytic formula:

$$\sigma_* = \sigma(k_{NL}^{-1} = R_*) \tag{15}$$

where $R_* = \sqrt{3}\sigma_1/\sigma_2$. $\sigma_j$ are the moments of the distribution of $\phi$ (Bardeen et al. 1986, Kofman 1989):

$$\sigma_j^2 = \frac{1}{2\pi^2} \int dk k^2 k^{2j} |\phi_k|^2. \tag{16}$$

The scale $R_*$ characterises the mean distance between peaks of the gravitational potential. For the truncated power law spectra considered by us: $k_c \times R_* \simeq \sqrt{6}$, 3, and 4, for $n = 1$, 0, and -1, respectively. For spectra having no built-in scale, the value of $R_*$ would be determined by the small scale cutoff introduced by the Nyquist frequency in a simulation.)

Fig. 10 shows the fraction of matter in caustics (stuck matter) $f(\sigma)$ (dotted curves), and the related underdensity of matter in voids $1 - f(\sigma)$ (solid curves) as a function of epoch, for the same set of simulations. Our simulations show that the rate of infall of matter into caustics is virtually insensitive to the spectral index in the range $-1 \leq n \leq +1$. We also find that by $\sigma(t) = \sigma_*$, virtually all of the matter is already in caustics, so that voids are relatively empty by this epoch (see also Pogosyan 1989, Sahni 1991). (The fraction of matter in caustics can be described to within 2% accuracy by the fitting function $f(\sigma) = \sigma^{3.6}(3 + \sigma^{3.6})^{-1}$ for $\sigma \geq 1$.)

Fig. 9b lends support to the viewpoint that the growth of large scale structure in the Universe is characterised by two complementary regimes. The first regime describes the formation of pancakes and the establishment of cellular structure ($\sigma(t) \leq \sigma_*$ during this period). However, the emergence of cellular structure in the Universe, is only an intermediate asymptote, and is succeeded by a second epoch during which large mass concentrations (knots and filaments) attract one another leading to the disruption of cellular structure at late times. As a result, whereas gravitational instability leads to pancaking during $\sigma(t) \leq \sigma_*$, hierarchical clustering characterises the later period $\sigma(t) > \sigma_*$. This interpretation is confirmed by a comparison of the results of 2D N-body simulations (Fig. 11 a-c) (Melott & Shandarin 1989; Beacom et al. 1991) with those of the adhesion model (Fig. 11 d-f). From Fig. 11 it is clear that the formation of cellular structure is complete by $\sigma = \sigma_* \simeq 4$ and that from then onwards clustering proceeds hierarchically. In fact, from Fig. 11 a-c and d-f we find that the number of voids first increases from one interconnecting void at $\sigma = 1$, to a maximum of eight voids at $\sigma = 4$ and then decreases to five voids at $\sigma = 16$. (We would like to add that despite the fact that gravitational clustering proceeds hierarchically during the second epoch ($\sigma(t) > \sigma_*$), we can still find the emergence of large correlated structures such as *secondary pancakes*, during this period, as has recently been demonstrated by Kofman et al. 1992.) This view of the formation and evolution of large scale structure is borne out by a study of the evolution of the void spectrum shown in Fig. 4 and Fig. 8a-d. From these figures we find that there are a greater number of large voids at early and late times. This clearly demonstrates that the evolution of voids proceeds in two distinct phases. During the first phase, ($\sigma(t) \leq \sigma_*$) large voids fragment into smaller voids. During the second phase, ($\sigma(t) > \sigma_*$), the reverse process takes place as voids begin to coalesce into larger units. The mean and maximum void sizes shown as functions of $\sigma(t)$ in Fig. 9a, provide further support to this point of view. Strictly speaking the above model assumes a cutoff in the initial spectrum as in our simulations. However, if the initial spectrum falls down as $k^{-3}$, as in the CDM model, then the evolution of the large scale structure also follows the above discription. The first caustics in this case are associated with the free-streaming distance for dark matter particles – in the case of a real (spatially unbounded) Universe, or with the artificial, Nyquist frequency cutoff – for a numerical simulation.

Finally, we would like to comment on the fact that the correlation of the height of the primordial potential with the void size appears to be more noticeable at late times when $\sigma > \sigma_*$ (see Fig. 5 and 6). The reason again lies in the fact that the formation of cellular structure is complete only by $\sigma \simeq \sigma_*$, where $\sigma_* \simeq 5$ for the power law spectra discussed in the previous paragraph. Therefore at earlier times when $\sigma \leq \sigma_*$ large voids are still in a state of *becoming*, since what used to be a large void at an early epoch gets fragmented into several smaller voids at later times and vice-versa. As a result, at epochs prior to $\sigma \simeq \sigma_*$, no definite relation as yet exists between the sizes of large but transient voids, and the height of the gravitational potential within them. At very late times the gravitational potential at the centres of voids is very nearly uniform irrespective of their size. (We should also note that since there are very few large voids in a given simulation, their distribution is plagued by small number statistics as evident from Fig. 5 and 6.)

## IV. SUBSTRUCTURE WITHIN VOIDS

A central result of our study of voids is that voids can be populated by substructures such as minipancakes and filaments which run through a void. Tis result emerges from a study of the topology of voids in Lagrangian space. The topology of a compact manifold, can be characterised by its genus measure $g$ which is related to the integrated Gaussian curvature $K$ of the manifold, by the Gauss-Bonnet formula

$$\oint K \, dA = 4\pi \, (1 - g) \tag{17a}$$

(For a sphere $K = r^{-2}, A = 4\pi r^2$, and therefore $g = 0$.) The genus is related to the Euler characteristic of a manifold $\kappa$, by the simple relation $g = 1 - \kappa/2$. At an intuitive level, we might say that the genus characteristic provides a measure of the number of holes in a given manifold. Thus, a sphere has genus $= 0$, a torus *genus* $= 1$, a pretzel *genus* $= 2$, and so on. In our present discussion we shall be interested in evaluating the topology of voids defined on a discrete grid in Lagrangian space. To do this we shall find it convenient to work with the discrete analog of the Gauss-Bonnet formula:

$$\sum_i D_i = 4\pi(1 - g). \tag{17b}$$

Here $D_i$ is the angle deficit defined at each vertex of the polyhedral void. Equation (17b) can be derived from equation (17a) if we note that all of the curvature of a discrete surface is localised in each of its $N$ vertices so that

$$K(x) \simeq \sum_i D_i \delta(x - x_i)$$

and

$$\oint K d^2x \simeq \oint \sum_i D_i \delta(x - x_i) d^2x = \sum_{i=1}^{N} D_i.$$

We apply equation (17b) to determine the topology of individual voids defined in L-space using the adhesion ansatz. (We would like to stress that, throughout the present discussion, the topology that is referred to will be that of *individual* voids, as opposed to the topology characterising large scale structure as a whole. See Melott 1990 for a comprehensive review of the subject of the topology of large scale structure.)

One of the most important results to emerge from the present analysis of voids using the adhesion model, is that voids in L-space can have a nontrivial topology. (We would like to point out in this context that the 2 dimensional L-space voids shown in Fig. 2c and Fig. 11 e,f, are all homomorphic to circles and have therefore an essentially trivial $S^1$ topology. In contrast to this the voids appearing in our three dimensional simulations sometimes show appreciable departures from a purely spherical (i.e., $S^2$) topology.) To illustrate what we mean, we plot one of the several topologically nontrivial void configurations that appear in our simulations in Fig. 12. The void has the topology of a torus in L-space i.e., the *free region* defining the void has a single hole (corresponding to stuck particles) passing through it. As mentioned in section 2 of this paper, the Euler picture of the distribution of caustics can be constructed from the coresponding Lagrangian picture, by moving the border between stuck and free regions by means of the Zeldovich approximation. This essentially amounts to moving the boundary of a void in L-space by the Zeldovich prescription (1). Since the Zeldovich approximation is a topology preserving transformation (Shandarin & Zeldovich 1989), it follows that a non-simply connected void in L-space will be mapped onto a topologically non-trivial configuration in E-space. In particular, a void having the topology of a torus (i.e., *genus* = 1), will correspond to a void having *one* minor Zeldovich pancake running through it. In general, a void in L-space having *genus* = $N_g$, will correspond in E-space, to $N_g$ minor Zeldovich pancakes running through a void bounded by major Zeldovich pancakes. (Observationally, such voids might convey the impression of being sponge-like.) We also feel that mini-pancakes within voids, could be young transient features, since our simulations show that voids tend to empty out with time, leading to a bubble like topology for voids at late times. The dynamical mechanism leading to the trivialisation of the void topology could be the following: As voids expand they empty out with time and matter from within them falls into pancakes (both mini as well as major). As a result, mini pancakes within voids evolve with time growing progressively more massive. At a later epoch these minor pancakes graduate into major Zeldovich pancakes and succeed in dynamically dividing a topologically nontrivial void into two or more topologically trivial voids. In order to estimate the evolution of the

void topology with time, we determine the mean genus characteristic of all voids $V_i$ in a given simulation

$$\bar{g}(\sigma) = \frac{1}{N} \sum_{i=1}^{N} g\,(V_i) \tag{18}$$

$N$ being the total number of voids at a given epoch.

The results of our simulations for the CDM model, are shown in Fig. 13 and 14. In Fig. 13 we plot the histogram of the genus per void against void size for three different epochs. What is plotted is $\langle g_i \rangle$ – the total genus of all voids in a certain class divided by the number of voids in that class:

$$\langle g_i \rangle = \frac{1}{n_i} \sum_{k=1}^{n_i} g_k,$$

where $n_i$ is the number of voids in the diameter class $D_i$ and $g_k$, $k = 1, \ldots, n_i$, are the genus values of the individual voids in that class. This is a good estimator of genus as a function of void diameter since the number of voids in different classes are different. In Fig. 14 we plot the mean genus in our simulation as a function of $\sigma(t)$. These two figures reveal that one out of every fourteen voids today has a nontrivial topology. By contrast, every eighth void had a topology that was nontrivial at a redshift of unity. Fig. 14 clearly demonstrates how the void topology evolves and essentially trivialises with time. A good analytical approximation to the time evolution of the mean genus, shown in Fig. 14 for the CDM model, is provided by $\bar{g}(\sigma) \propto \sigma^{-3/2}(t)$. For comparison we also plot the genus, against void size and as a function of $\sigma(t)$, for the power law spectra $P(k) = \langle |\delta_k|^2 \rangle \propto k^n$ for $k \leq k_c$, $P(k) = 0$ for $k > k_c$, $n = -1, 0, +1$, in Fig. 15, & 16, respectively. We find that in this case too, larger voids tend to have a more complicated topology than smaller voids, and that the overall void topology tends to simplify with time. It is interesting to note that some voids such as the Coma void, do indeed seem to be populated by mini-Zeldovich pancakes, as pointed out recently by Park et al. 1992.

From Fig. 13 we find that the ratio of the diameter of a void in Eulerian space to its diameter in Lagrangian space, grows very nearly as $D_E/D_L \propto \sigma(t)$, regardless of the size of the void. This relation is easy to understand if one notes that at late times equation (11) reduces to

$$\begin{aligned} V_E &= \sum_{i=1}^{N} dV_L \; [1 - a(t)\lambda_1(q_i)]\,[1 - a(t)\lambda_2(q_i)]\,[1 - a(t)\lambda_3(q_i)] \\ &\underset{a \gg 1}{=} - N dV_L \; a^3(t) \sum_{i=1}^{N} \frac{\lambda_1(q_i)\lambda_2(q_i)\lambda_3(q_i)}{N} \end{aligned} \tag{19}$$

so that,

$$\left(\frac{V_E}{V_L}\right)^{\frac{1}{3}} \equiv \frac{D_E}{D_L} = \sigma(t)\,\langle I_3\rangle^{\frac{1}{3}}\,,$$

where

$$\langle I_3\rangle = -\frac{1}{N}\sum_{i=1}^{N}\lambda_1(q_i)\lambda_2(q_i)\lambda_3(q_i),$$

is the mean value of the invariant $I_3$ in the given L-space void. $N$ denotes the number of *free* unit volume elements in a given L-space void, and $V_L = N \times dV_L$ is the Lagrangian volume of the void ($\sigma(t) \propto a(t)$). From Fig. 13 it follows that small voids in L-space remain small in E-space and vice versa. The ratio $V_L/V_E = (D_L/D_E)^3$ is a measure of the underdensity of voids. From this figure we find that

$$\left\langle \frac{V_L}{V_E} \right\rangle_{z=0} \simeq \frac{1}{8}\left\langle \frac{V_L}{V_E} \right\rangle_{z=1},$$

indicating that voids today are $\sim 8$ times more empty than they were at redshifts of unity. (Note that $\sigma \simeq 9$ today, for the COBE-normalised CDM model.)

## V. DISCUSSION

We have applied the adhesion model to determine the spectrum of void sizes, both for the COBE-normalised CDM model, as well as for models with power-law spectra $P(k) \propto k^n$, $n = -1, 0, +1$. The model neglects the volume occupied by clusters and superclusters, however it does not make any a priori assumptions on the geometry and topology of the voids. The advantage of the adhesion model is that it includes both dynamical as well as statistical aspects of void formation. We find that most of the characteristics of voids, such as the mean and maximum void size in a simulation, evolve with time. For the CDM model we find that $\bar{D} = \bar{D}_0/\sqrt{1+z}$, where $\bar{D}_0 \simeq 10.5$ Mpc, is the mean void size today. We also find that the total number of voids in a simulation, varies with cosmic epoch, increasing to a maximum value at $\sigma_* = \sigma(k_{NL}^{-1} = R_*)$, and then decreasing monotonically. We feel that the expansion scale $\sigma_*$ separates two distinct phases in gravitational instability. During the first phase ($\sigma \leq \sigma_*$), gravitational instability proceeds via the formation of pancakes, and the subsequent establishment of cellular structure, which is complete by $\sigma(t) = \sigma_*$. However, pancake formation happens to be an intermediate asymptote and during the second phase ($\sigma(t) > \sigma_*$) gravitational instability proceeds hierarchically, leading to the eventual disruption of cellular structure.

Our results show that the sizes of voids are stongly correlated with the height of the primordial gravitational potential at void centers, larger voids forming in regions where the gravitational potential is higher. This result indicates that knowing the observed form of the void spectrum it might be possible to, at least partially, reconstruct the primordial form

of the potential. Assuming the Harrison-Zeldovich initial spectrum one can easily verify that the gravitational potential is not a homogeneous random function if the spectrum is extrapolated to $k = 0$. It means that the largest void is probably determined by the size of a sample.

One of the most intriguing results of the present analysis is that voids can have a topology which is nontrivial. We find that the topology of a void depends upon its size, with larger voids more likely to have a nontrivial topology than smaller voids. We also find that the topology of voids, like the void spectrum evolves with time, with voids becoming progressively emptier at later times. Our results for the CDM model show that one out of every 14 voids is likely to have some substructure, such as a filament or a pancake passing through it. These results are supported by recent observations indicating the presence of galaxies (Westrop et al. 1992) and mini-pancakes (Park et al. 1992) within at least two voids. It is likely that with the advent of deeper and more complete redshift surveys the issue of void size and void substructure will take on a deeper significance, as a detailed picture of the texture of voids in the Universe emerges. Bearing this in mind, we believe that the topological indicator of void substructure developed by us in this paper, can emerge as a key statistical indicator for the study of voids in the Universe.

If both the shape and the amplitude of the initial perturbation spectrum are independantly known (for instance from the angular fluctuations of the cosmic microwave background radiation), then void statistics in the adhesion approximation is determined solely by the growth factor of the linear density contrast $D(z, \Omega)$ (which determines the curvature of the osculating paraboloid). In such a case the void spectrum can potentially be used to determine the value of $\Omega$.

In a companion paper we shall apply the void spectrum and topology measuring ansatz, developed in the present paper, to compare and contrast several cosmological scenario's, including "tilted" cold dark matter models, cold dark matter models with a cosmological constant, and models containing a mixture of cold + hot dark matter (Sahni, Sathyaprakash & Shandarin 1993).

Finally we would like to mention that the consistency of the results obtained in this paper was checked using the 3D adhesion code independently developed by Dima Pogosyan.

## Acknowledgements

We benefitted from discussions with Dick Bond, Hugh Couchman, Bala Iyer, Chanda Jog, Nick Kaiser, Henry Kandrup, Lev Kofman, Blane Little, Adrian L. Melott, Jayant Narlikar and John Peacock. We are grateful to Dima Pogosyan for sharing with us his adhesion code and for clarifying a number of conceptual issues. One of us (BSS) would like to thank Abdus Salam, the International Atomic Energy and UNESCO for hospitality

at the International Centre for Theoretical Physics, Trieste where a part of this work was carried out. BSS would also like to thank Dennis Sciama for encouragement. One of the authors (S.F.Sh.) acknowledges NASA grant NAGW-2923, NSF grants AST-9021414 and OSR-9255223, and the University of Kansas GRF fund for financial support.

## REFERENCES

Bardeen, J.M., Bond, J.R., Kaiser, N., & Szalay, A.S. 1986, ApJ, 304, 15.

Beacom, J.F., Dominik, K.G., Melott, A.L., Perkins, S.P., & Shandarin, S.F. 1991, ApJ, 372, 351

Bertschinger, E. 1985, ApJS, , 58, 1

Blaes, O., Villumsen, J. V., & Goldreich, P. 1990, ApJ, 361, 331

Blumenthal, G. R., da Costa, L. N., Goldwirth, D. S., Lecar, M., & Piran, T. 1992, ApJ, 388, 234

Bonnor, W. B., & Chamorro, A. 1990, ApJ, 361, 21

Broadhurst, T. J., Ellis, R. S., Koo, D. C., & Szalay, A. S. 1990, Nature, 343, 726

Burgers, J. M. 1974, The Nonlinear Diffusion Equation (Dordrecht: Reidel)

Davis R. L., Hodges, H. M., Smoot, G. F., Steinhardt, P. J., & Turner, M. S. 1992, Phys. Rev. Lett., 69, 1856

Dubinski, J., da Costa, L. N., Goldwirth, D. S., Lecar, M., & Piran, T. 1993, to appear in ApJ

Efstathiou, G., Bond, J. R., & White, S. D. M. 1992, MNRAS, 258, p1

Fillmore, J. A., & Goldreich, P. 1984, ApJ, 281, 9

Gurbatov, S. N., Saichev, A. I., & Shandarin, S. F. 1985, Soviet Phys. Dokl. 30, 921

Gurbatov, S. N., Saichev, A. I., & Shandarin, S. F. 1989, MNRAS, 236, 385

Harrington, P. M., Melott, A. L., & Shandarin, S. F. 1993, in preparation

Hausman, M. A., Olson, D. W., & Roth, B. D. 1983, ApJ, 270, 351

Hoffman, G. L., Salpeter, E. E., & Wasserman, I. 1983, ApJ, 268, 527

Icke, V. 1984, MNRAS, 206, 1p

Icke, V., & Van de Weygaert, R. 1987, A&A, 184, 16

Kauffmann G., & Fairall, A. P. 1991, MNRAS, 248, 313

Kauffmann G., & Melott, A. L. 1992, ApJ, 393, 415

Kirshner, R. P., Oemler, A. Jr., Schechter, P. L., & Shectman, S. A. 1981, ApJ, 248, L57

Kofman, L. A. 1989, in Lecture Notes in Physics, 332, Morphological Cosmology, ed. P. Flin, & H. W. Duerbeck (Berlin: Springer-Verlag) 354

Kofman, L. A. 1991, in Primordial Nucleosynthesis and Evolution of Early Universe, ed. K. Sato, & J. Audouze (Dordrecht: Kluwer) 495

Kofman, L. A., Pogosyan, D. Yu., & Shandarin, S. F. 1990, MNRAS, 242, 200

Kofman, L. A., Pogosyan, D. Yu., Shandarin, S. F., & Melott, A. L. 1992, ApJ, 393, 437

Kofman, L. A., & Shandarin, S. F. 1988, Nature, 334, 129

de Lapparent, V., Geller, M. J., & Huchra, J. P. 1986, ApJ, 302, L1

Liddle, A. R., & Lyth, D. H., 1992, Phys. Lett., B291, 391

Lidsey, J. E., & Coles, P. 1992, MNRAS, 258, 57p

Lin, C. C., Mestel, L., & Shu, F. H. 1965, ApJ, 142, 1431

Little, B. 1992, private communication

Lucchin, F., Mataresse, S., & Mollerach, S. 1992, ApJ, 401, L49

Melott, A. L. 1990, Physics Reports 193, 1

Melott, A. L., & Shandarin, S. F. 1989, ApJ, 343, 26

Melott, A. L., & Shandarin, S. F. 1993, ApJ, 410, 469

Nusser, A., & Dekel, A. 1990, ApJ, 362, 14

Park, C., Gott, J. R., Melott, A. L., & Karachentsev, I. D. 1992, ApJ, 387, 1

Peebles, P. J. E. 1982, ApJ, 257, 438

Piran, T., Lecar, M., Goldswirth, D.S., da Costa, L.N. and Blumenthal, G.R., 1993, MNRAS, , **265**, 681.

Pogosyan, D. Yu. 1989, Tartu preprint (Estonian Acad. Sci.)

Regos, E., & Geller, M. J. 1991, ApJ, 377, 14

Sahni, V. 1991, in Annals of the New York Academy of Sciences, 647, Proceedings of the Texas/ESO-CERN symposium on Relativistic Astrophysics, Cosmology and Fundamental Physics, 749

Sahni, V., & Souradeep, T. 1992, to appear in The Proceedings of the First Iberian Meeting on Gravity, September 21 - 27, 1992, Evora, Portugal, ed. M. Bento, O. Bertolami, & J. Mourao (Singapore: World Scientific)

Sahni, V., Sathyaprakash, B. S., & Shandarin, S. F. 1993, in preparation

Salopek, D. S. 1992, Phys. Rev. Lett., 69, 3602

Shandarin, S. F., & Zeldovich, Ya. B. 1989, Rev. Mod. Phys., 61 185

Slezak, E., de Lapparent, V., & Bijaini, A. 1993, ApJ, 409, 517

Smoot, G.F. et al. 1992, ApJ, 396, L1

Souradeep, T., & Sahni, V. 1992, Mod. Phys. Lett., A7, 3541

van de Weygaert, R., 1991, Voids and Geometry of the Large Scale Structure, PhD thesis
van de Weygaert, R., & van Kampen, E. 1993, MNRAS, 263, 481

Vogeley, S. V., Geller, M. J., & Huchra, J. P. 1991, ApJ, 382, 44

Weinberg, D., & Gunn, J. 1990, MNRAS, 247, 260

Weistrop, D., Hintzen, P., Kennicutt, R. C., Liu, C., Lowenthal, J., Cheng, K. P., Oliverson, R., & Woodgate, B. 1992, ApJ, 396, L23

Williams, B. G., Heavens, A. F., Peacock, J. A., & Shandarin, S. F. 1991, MNRAS, 250, 458

Zeldovich, Ya. B. 1970, A&A, 5, 84

Zeldovich, Ya. B., Einasto, J., & Shandarin, S. F. 1982, Nature, 300, 407

Zeldovich, Ya. B., & Shandarin, S. F. 1982, Sov. Astron. Lett., 8, 67

## FIGURE CAPTIONS

**Fig. 1**

The geometrical prescription of descending a paraboloid onto the gravitational potential in order to demarcate *stuck* and *free* Lagrangian regions, is shown in one dimension. The peaks of the potential correspond to regions where the eigenvalue $\lambda < 0$. The particle having Lagrangian coordinate $q_0$ is free in the uppermost figure, and has just entered into a caustic in the middle figure. The middle and lower figures describe the merger of clumps.

**Fig. 2**

The distribution of caustics (dots) (for two-dimensional simulations) is plotted superimposed on *free* (shaded) and *stuck* (unshaded) Lagrangian regions for three distinct expansion epochs: (a) $\sigma(t) = 1$, (b) $\sigma(t) = 2$, and (c) $\sigma = 8$. (d) Results of two-dimensional N-body simulations are shown for the epoch $\sigma(t) = 2$ (Melott & Shandarin 1989). (e) Particles evolved according to the Zeldovich approximation are shown for $\sigma(t) = 2$.

**Fig. 3**

Regions in Lagrangian space where both the eigenvalues of the two-dimensional deformation tensor are negative, are shown (dotted regions). Also shown superimposed are voids in Lagrangian space obtained using the adhesion model, for the same spectrum, at very late times (shaded regions).

**Fig. 4**

The void spectrum for the COBE - normalised CDM model, is plotted for three time scales: (top) the past $a = 0.5\ a_0, z = 1$; (center) the present $a = a_0, z = 0$; and (bottom) the future (!) $a = 1.5\ a_0$; ($a$ – is the expansion factor, and $z$ the redshift). In all the pictures the x-axis is an indicator of the void diameter in Mpc. The left hand pictures illustrate the volume fraction of voids having a given diameter "$D$" (in Mpc) $v(D)/V$ sometimes called the *void spectrum.* ($v(D)$ is the volume occupied by voids in a bin of size $D \pm 2$ Mpc and $V$ is the total volume occupied by all voids which, in the adhesion model, is equal to the volume of the simulation box.) The right hand pictures show the corresponding number fraction of voids, also plotted against the void diameter. The error bars in these histograms correspond to *rms* dispersion over three simulations. We would like to point out that the number of large voids in a given simulation is too small to be resolved in the number fraction histogram. Their presence is, however, seen in the void spectrum.

**Fig. 5**

The value of the normalised primordial gravitational potential ($\phi/\phi_{rms}$) evaluated at the centers of voids is shown plotted against the void diameter for the present epoch for one realisation of the COBE - normalised CDM spectrum.

**Fig. 6**

The value of the normalised primordial gravitational potential ($\phi/\phi_{rms}$) evaluated at the centers of voids is shown plotted against the void diameter for power law primordial spectra $P(k) \propto k^n$, for $k < k_c$; $P(k) = 0$, for $k \geq k_c$, where $k_c = 16 \times k_f$, $k_f = 2\pi/L_{box}$, is the wavenumber of the fundamental mode. The figures (top to bottom) correspond to three different cosmic expansion epochs: $\sigma = 4$, $\sigma = 8$, and $\sigma = 16$. From left to right the figures correspond to $n = 1$, (left column) $n = 0$ (middle) and $n = -1$ (right).

**Fig. 7**

The growth of $\langle\phi(t)\rangle/\phi_{rms}$ is shown plotted against the cosmic expansion factor $\sigma(t)$, for two of the three power law spectra discussed in the previous figure: $n = 1$ (solid line) and $n = 0$ (dashed line).

**Fig. 8**

(a) The void spectrum $v(D)/V$ is plotted against the void diameter $D$, for the truncated power law spectrum of Fig. 6, 7 with spectral index $n = 1$ and for nine different expansion epochs. (b) The number fraction of voids $n(D)/N$ is plotted against the void diameter $D$ for the power law spectrum and expansion epochs of Fig. 8a. (c) The void spectrum $v(D)/V$ (left) and the void number fraction $n(D)/N$ (right) are plotted against the void diameter $D$ for the truncated power law spectrum of Fig. 6, 7 with spectral index $n = 0$ and for three different expansion epochs. (d) The same as Fig. 8c but with spectral index $n = -1$.

**Fig. 9**

(a) The time evolution of the mean (left panel) and maximum (right panel) void diameters, in our simulation cube, are shown as functions of $\sigma(t)$ for the same power law primordial spectra as in the previous figure: $n = 1$ (solid line), $n = 0$ (dashed line), $n = -1$ (dotted line). The error bars indicate the *rms* dispersion from three simulations. (b) The time evolution of the total number of voids in our simulation cube, is shown as a function of $\sigma(t)$ for the same power law primordial spectra as in the previous figure: $n = 1$ (solid line), $n = 0$ (dashed line), $n = -1$ (dotted line). The error bars indicate the *rms* dispersion from three simulations.

**Fig. 10**

The fraction of matter in caustics (dotted curves) and the corresponding underdensity of matter in voids (solid curves) are shown as functions of the expansion factor $\sigma(t)$, for the power law primordial spectra previously considered. (The upper (lower) dotted curve and the lower (upper) solid curve correspond to $n = -1$ ($n = 1$).) The dispersion resulting from different simulations is so small that it cannot be resolved in this graph. Also, the curves are virtually insensitive to the index of the power spectrum.

**Fig. 11**

Results for two-dimensional N-body simulations involving $512 \times 512$ particles, are shown for different instants of time corresponding to: $(a)$ $\sigma(t) = 1$, $(b)$ $\sigma(t) = 4$ and $(c)$ $\sigma(t) = 16$. The primordial power spectrum for these simulations was assumed to be a truncated power law: $P(k) \propto k^2$ for $k < k_c, P(k) = 0$ for $k \geq k_c$, where $k_c = 4 \times k_f$, $k_f$ being the fundamental frequency $k_f = 2\pi/L_{box}$. (Melott & Shandarin 1989.) Voids in L-space (described by shaded regions) evaluated using the adhesion approximation are shown for initial conditions and epochs identical to those in Fig. 11 a-c: (d) $\sigma(t) = 1$, (e) $\sigma(t) = 4$, and (f) $\sigma(t) = 16$.

**Fig. 12**

A topologically nontrivial void in Lagrangian space having genus = 1 is shown from our CDM simulations.

**Fig. 13**

In the left hand pictures, the mean genus of voids belonging to a given diameter class $\langle g_i \rangle$, is shown plotted against the void diameter in Lagrangian space – $D_L$, for simulations involving the CDM model, and for the same expansion epochs as in Figure 5 (i.e., from top to bottom: $a/a_0 = 0.5, 1, 1.5$). The corresponding Euler diameters of voids, $D_E$, are shown plotted against the Lagrangian diameters $D_L$, in the right hand pictures. The solid line corresponds to $D_E/D_L = \sigma(t)\langle|\lambda_1\lambda_2\lambda_3|\rangle^{\frac{1}{3}}$, which is a constant for a given simulation.

**Fig. 14**

The mean genus characteristic evaluated for the entire ensamble of voids in the CDM model, is shown for the expansion epochs: $a/a_0 = 0.5, 1, 1.5$, corresponding to the past ($z = 1$), the present ($z = 0$), and the future.

**Fig. 15**

Same as Fig. 13 but for power law spectra $P(k) \propto k^n, k < k_c; P(k) = 0, k \geq k_c$, where $k_c = 16 \times k_f$, $k_f = 2\pi/L_{box}$, is the wavenumber of the fundamental mode: (a) $n = 1$, (b) $n = 0$, and (c) $n = -1$.

**Fig. 16**

Same as Fig. 14 but for the power law spectra of Fig. 15.

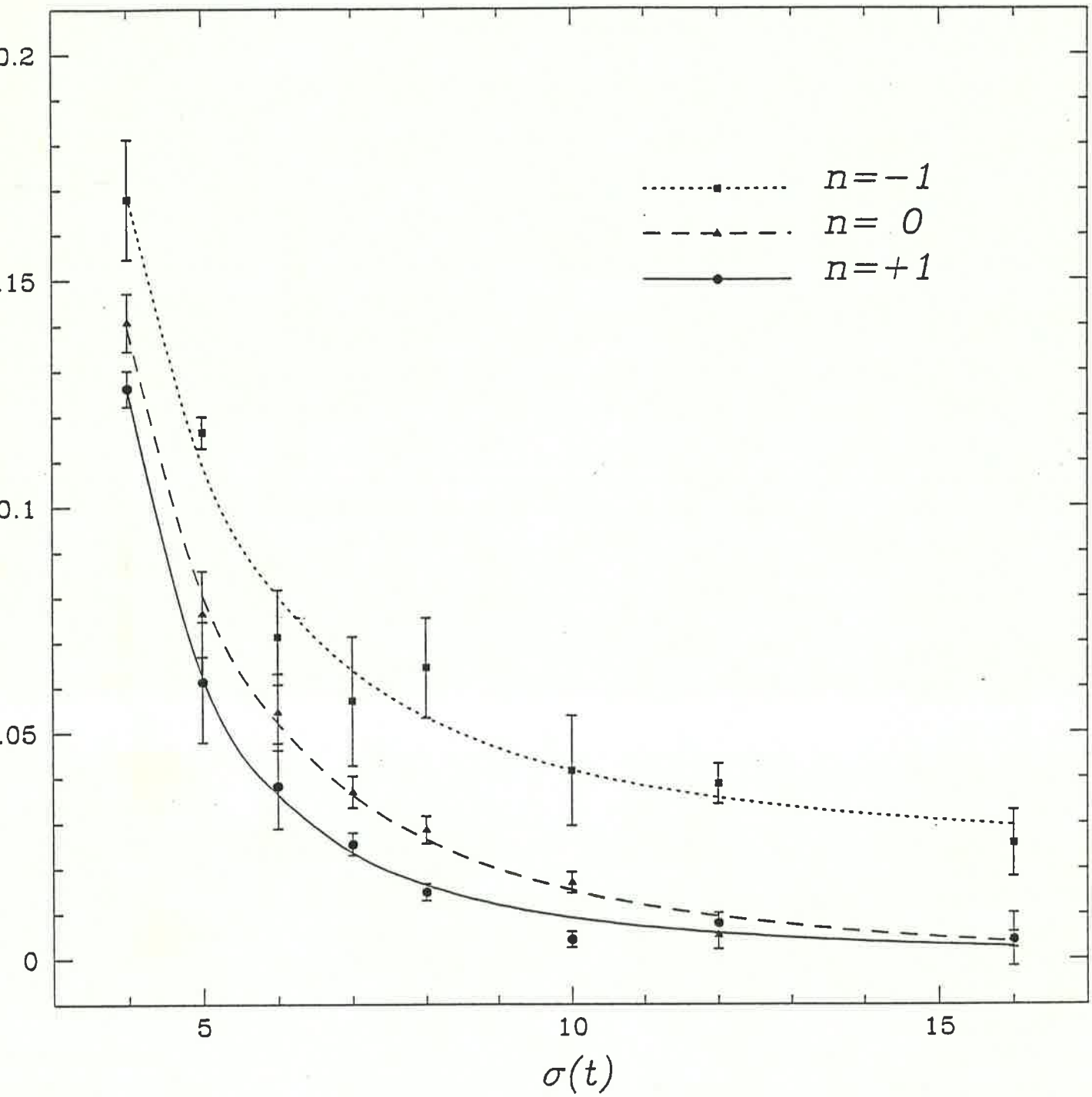


Fig. 16

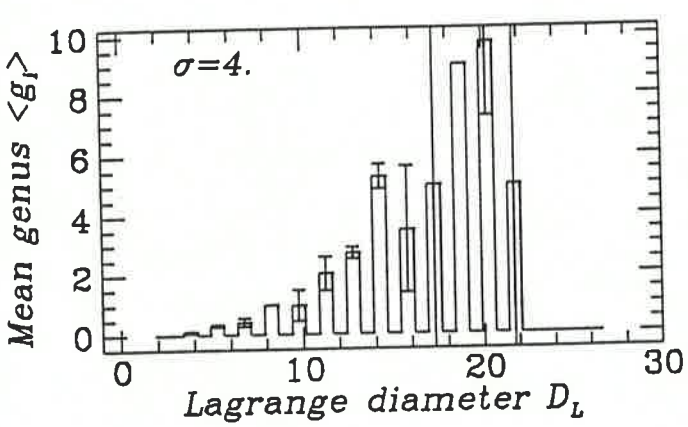
σ=4.
Mean genus <g_l>
Lagrange diameter D_L

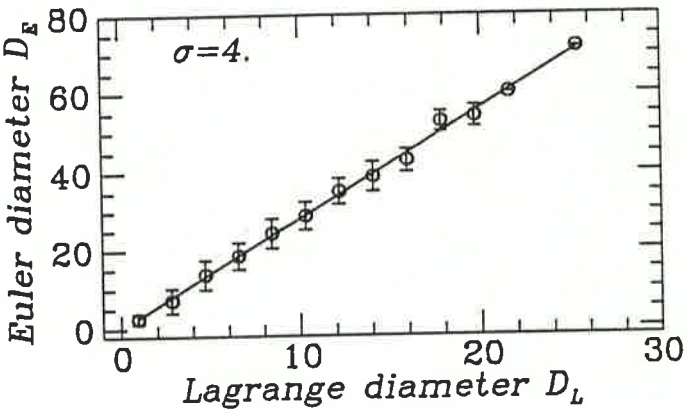
σ=4.
Euler diameter D_E
Lagrange diameter D_L

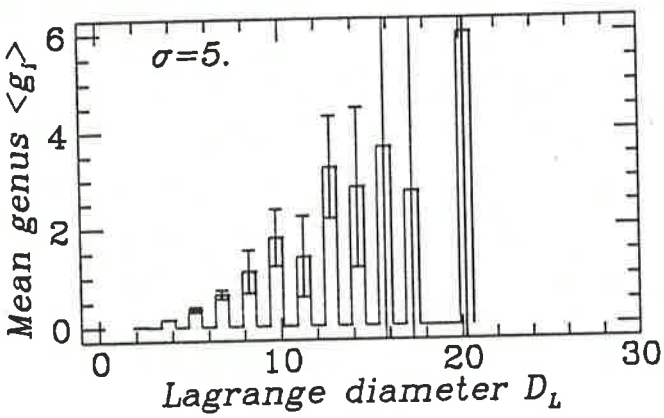
σ=5.
Mean genus <g_l>
Lagrange diameter D_L

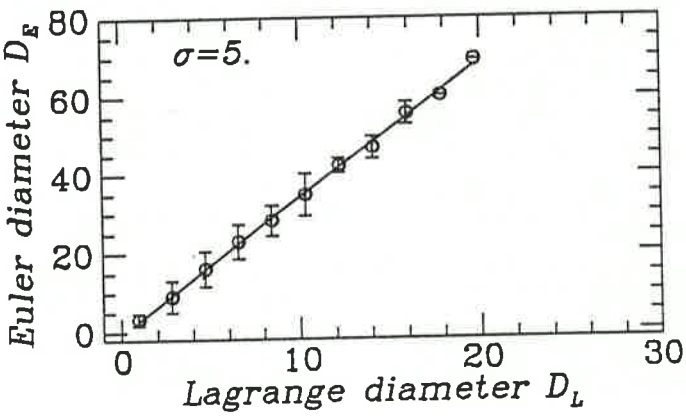
σ=5.
Euler diameter D_E
Lagrange diameter D_L

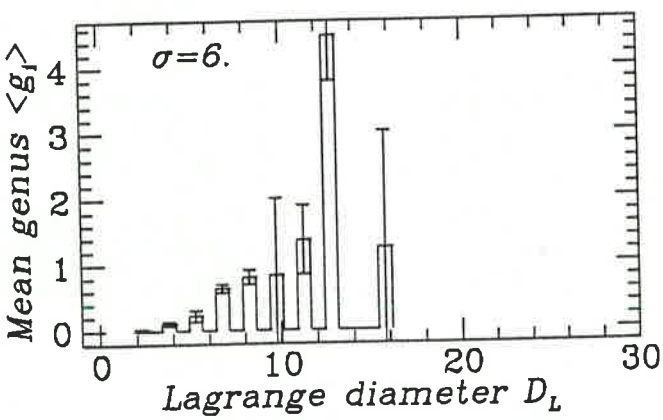
σ=6.
Mean genus <g_l>
Lagrange diameter D_L

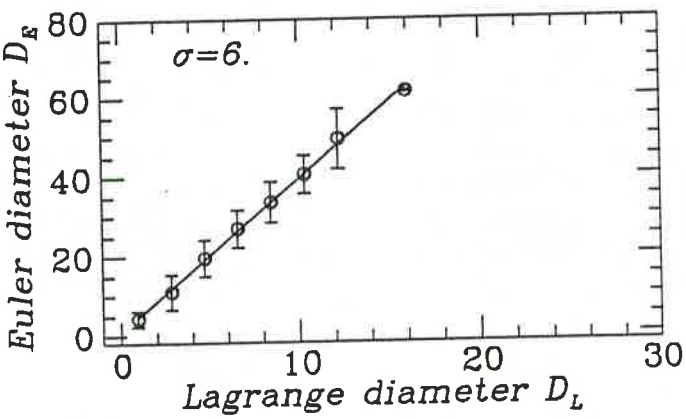
σ=6.
Euler diameter D_E
Lagrange diameter D_L

Fig. 15c

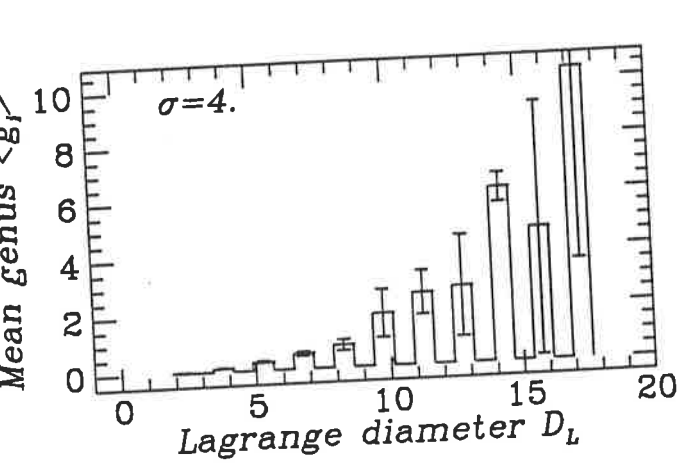
Mean genus <g_f>
σ=4.
Lagrange diameter D_L

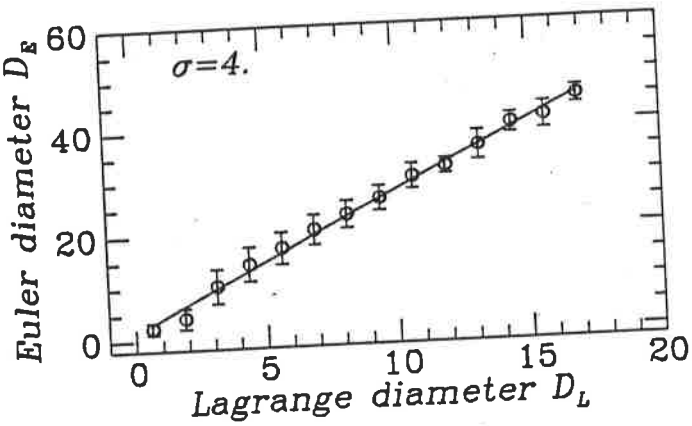
Euler diameter D_E
σ=4.
Lagrange diameter D_L

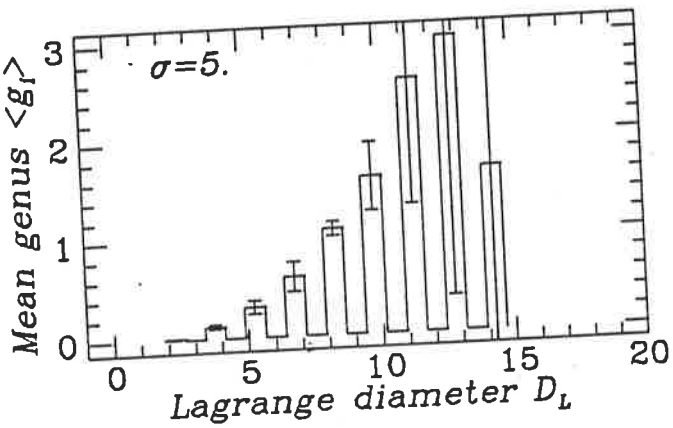
Mean genus <g_f>
σ=5.
Lagrange diameter D_L

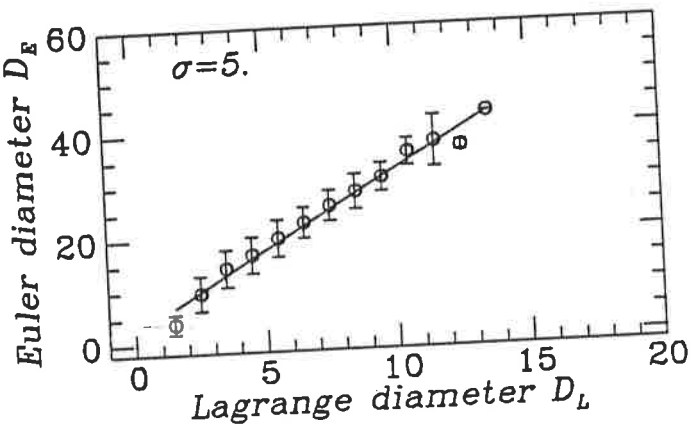
Euler diameter D_E
σ=5.
Lagrange diameter D_L

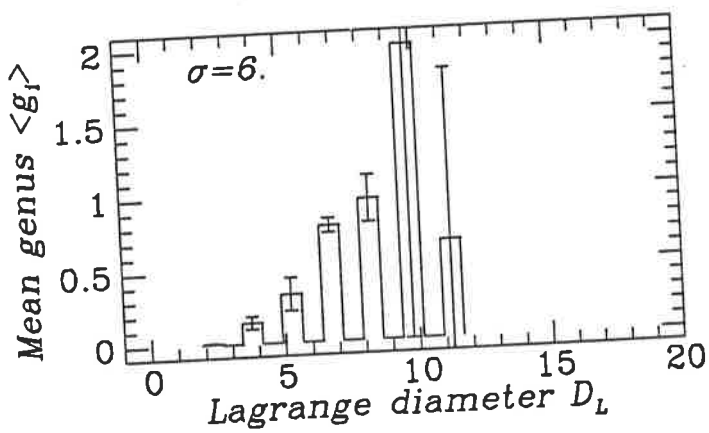
Mean genus <g_f>
σ=6.
Lagrange diameter D_L

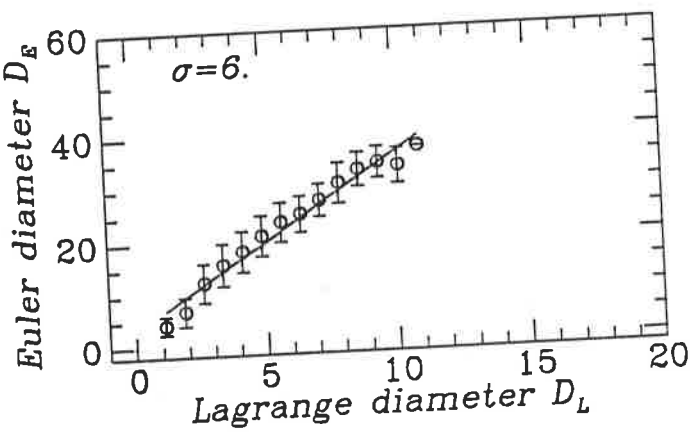
Euler diameter D_E
σ=6.
Lagrange diameter D_L

Fig. 15b

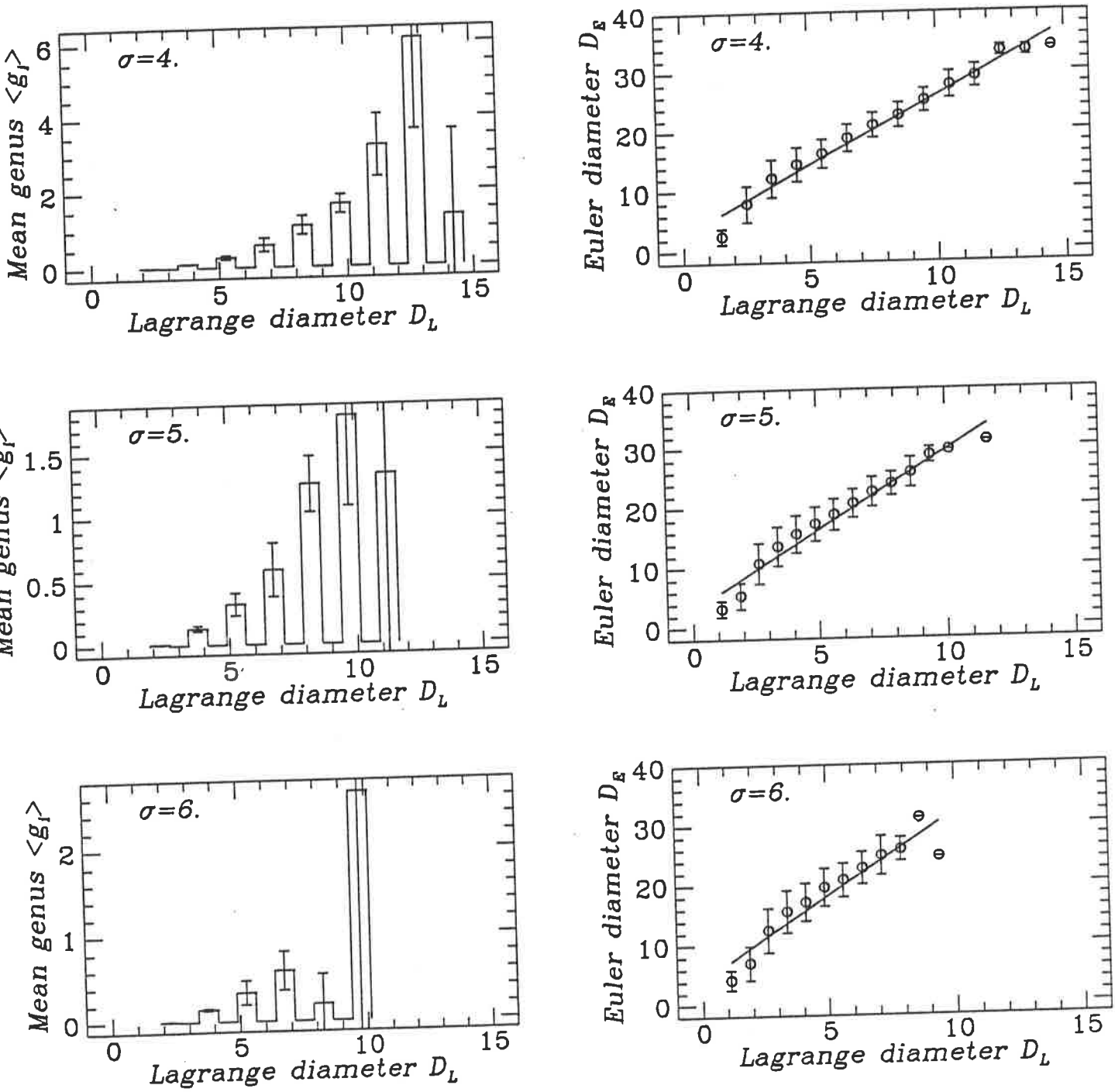
σ=4.
Mean genus <g_l>
Lagrange diameter D_L
Euler diameter D_E
σ=5.
σ=6.

Fig. 15a

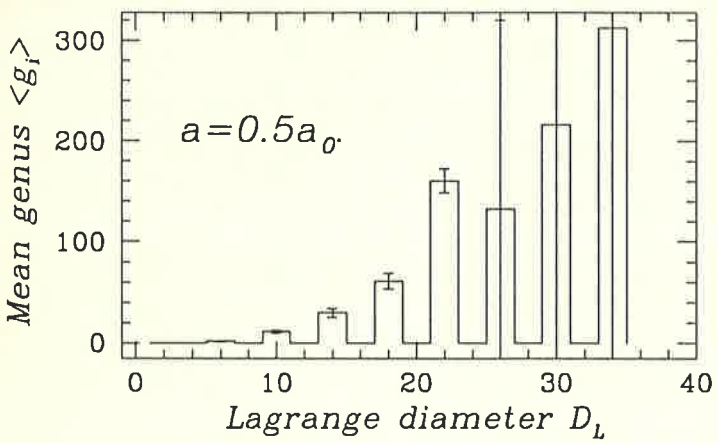
Mean genus $\langle g_i \rangle$
300
200
100
0
$a=0.5a_0$
0
10
20
30
40
Lagrange diameter $D_L$

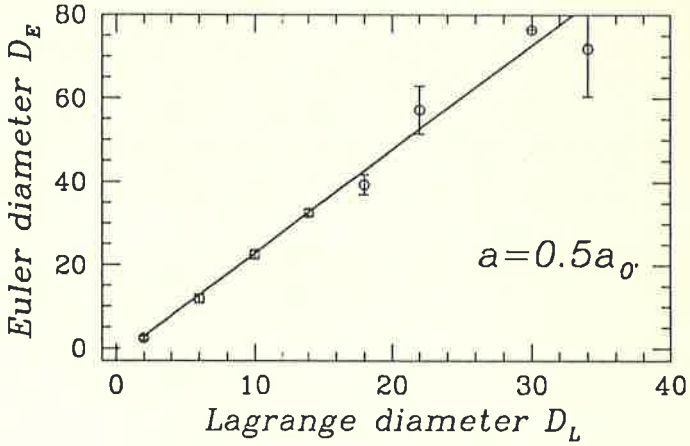
Euler diameter $D_E$
80
60
40
20
0
$a=0.5a_0$
0
10
20
30
40
Lagrange diameter $D_L$

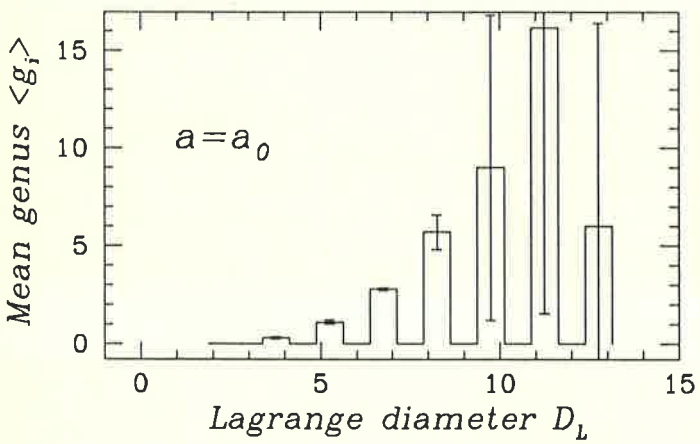
Mean genus $\langle g_i \rangle$
15
10
5
0
$a=a_0$
0
5
10
15
Lagrange diameter $D_L$

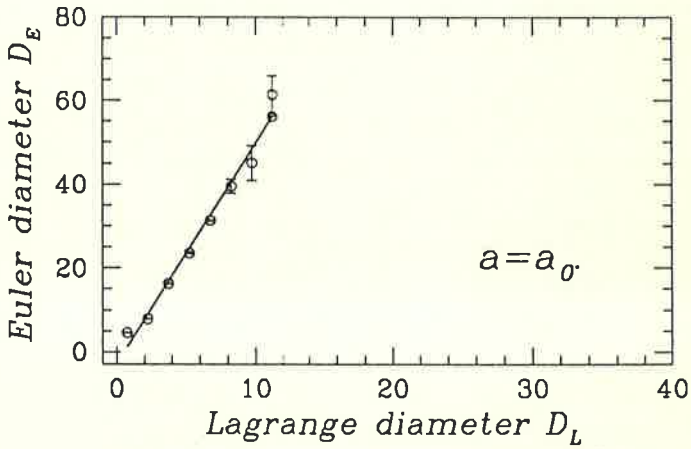
Euler diameter $D_E$
80
60
40
20
0
$a=a_0$
0
10
20
30
40
Lagrange diameter $D_L$

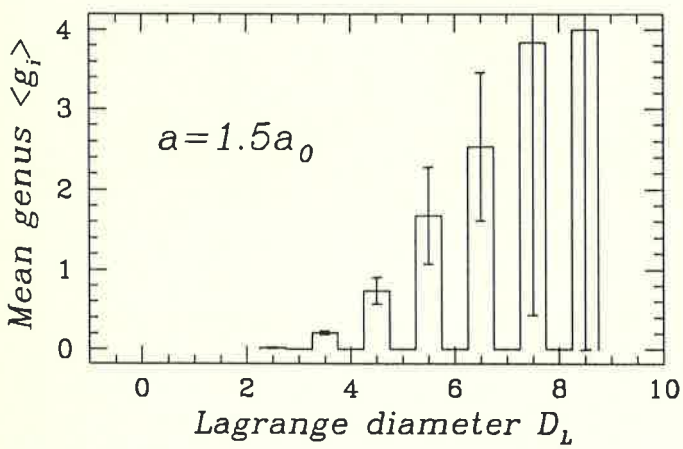
Mean genus $\langle g_i \rangle$
4
3
2
1
0
$a=1.5a_0$
0
2
4
6
8
10
Lagrange diameter $D_L$

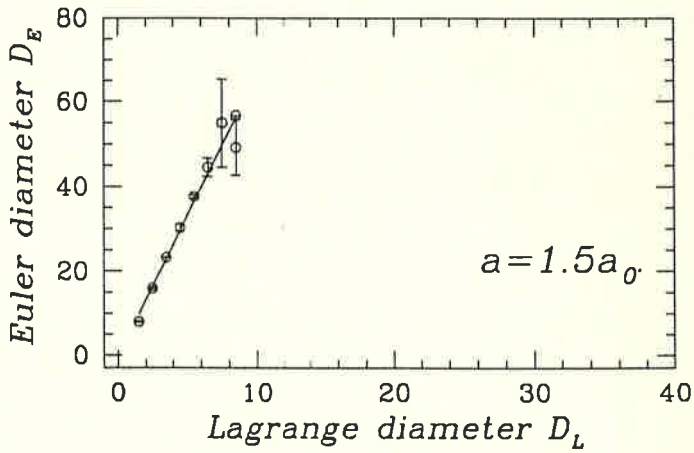
Euler diameter $D_E$
80
60
40
20
0
$a=1.5a_0$
0
10
20
30
40
Lagrange diameter $D_L$

Fig. 13

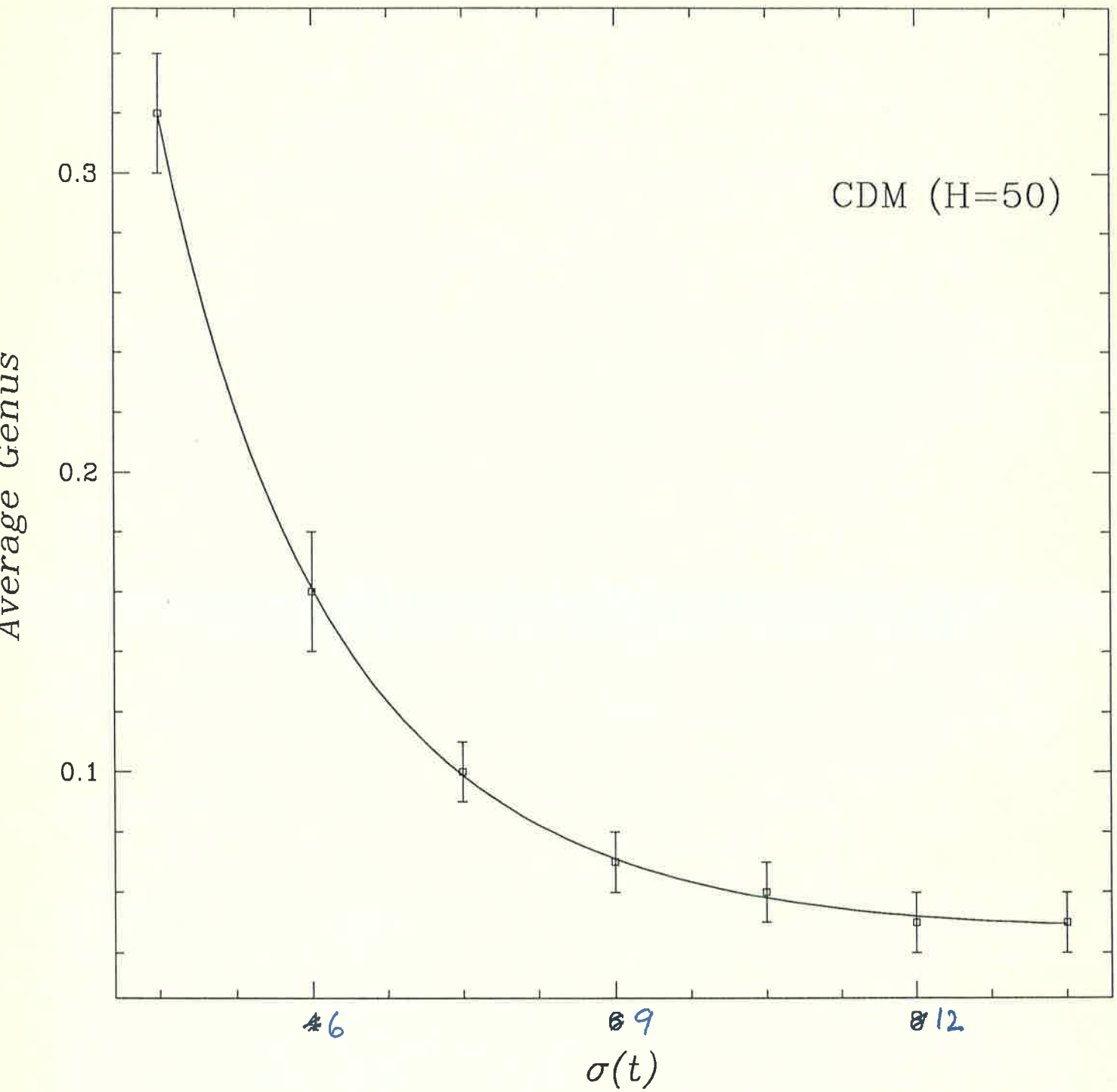


Fig. 14

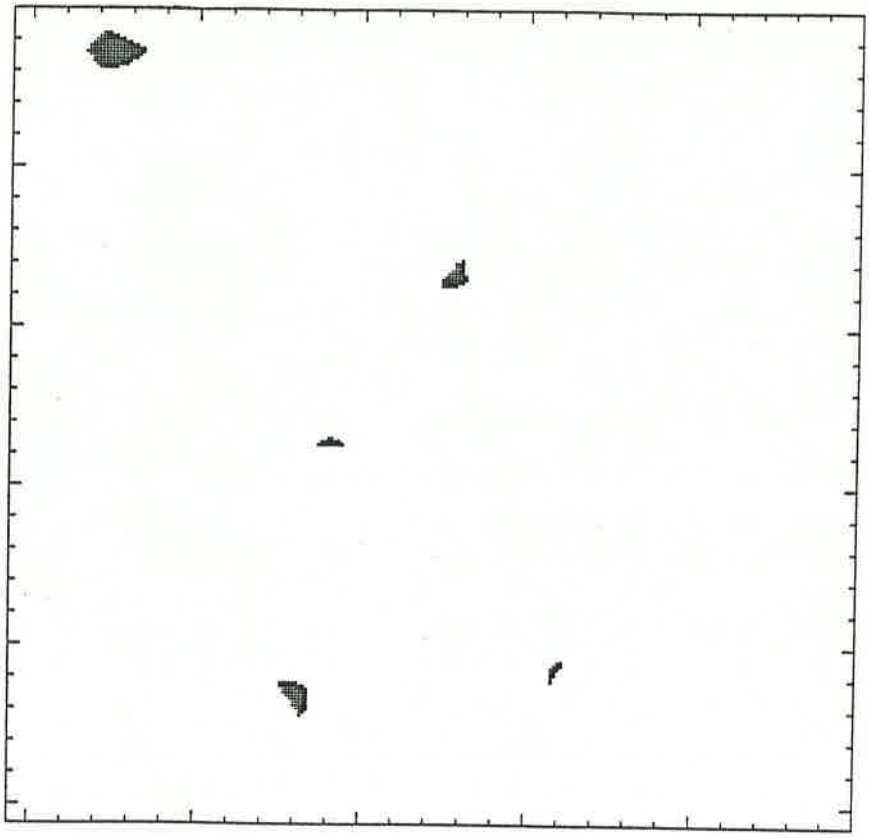

Fig. 11f

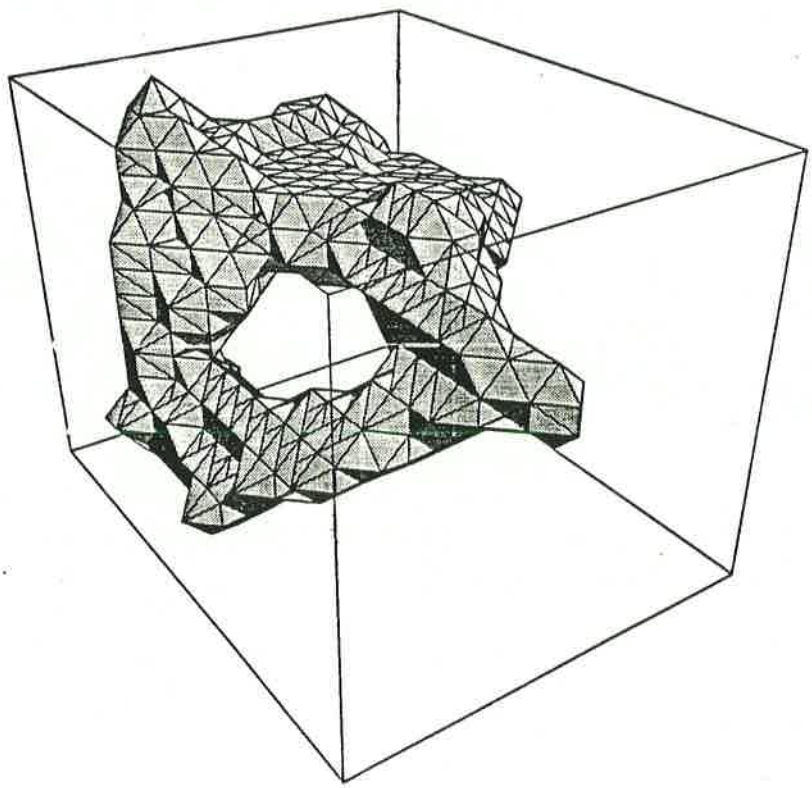

Fig. 12

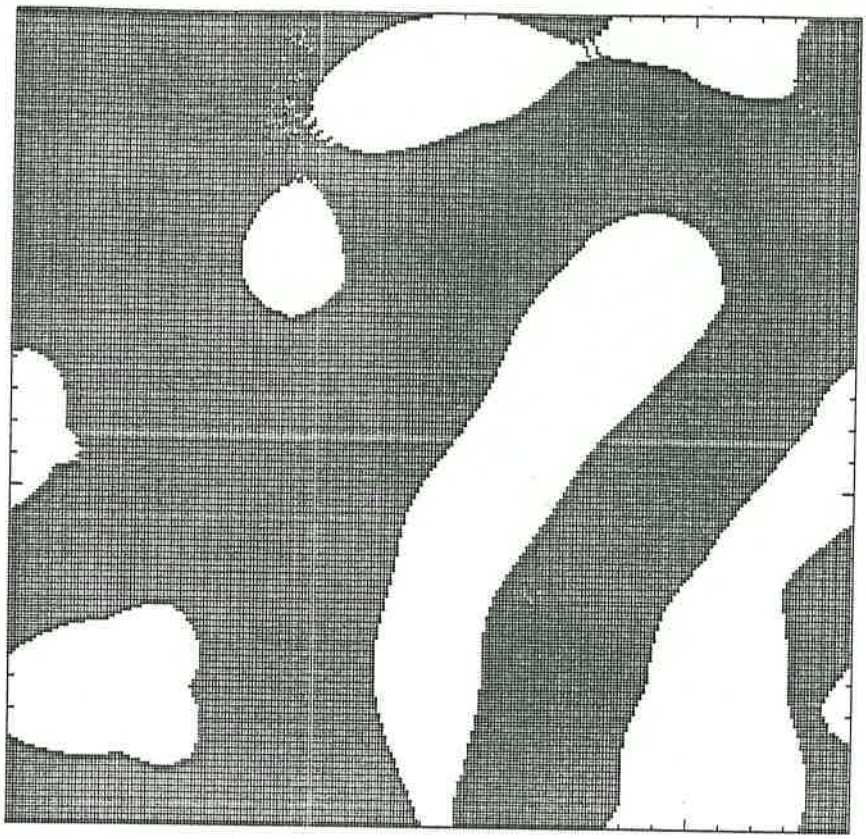

Fig. 11d

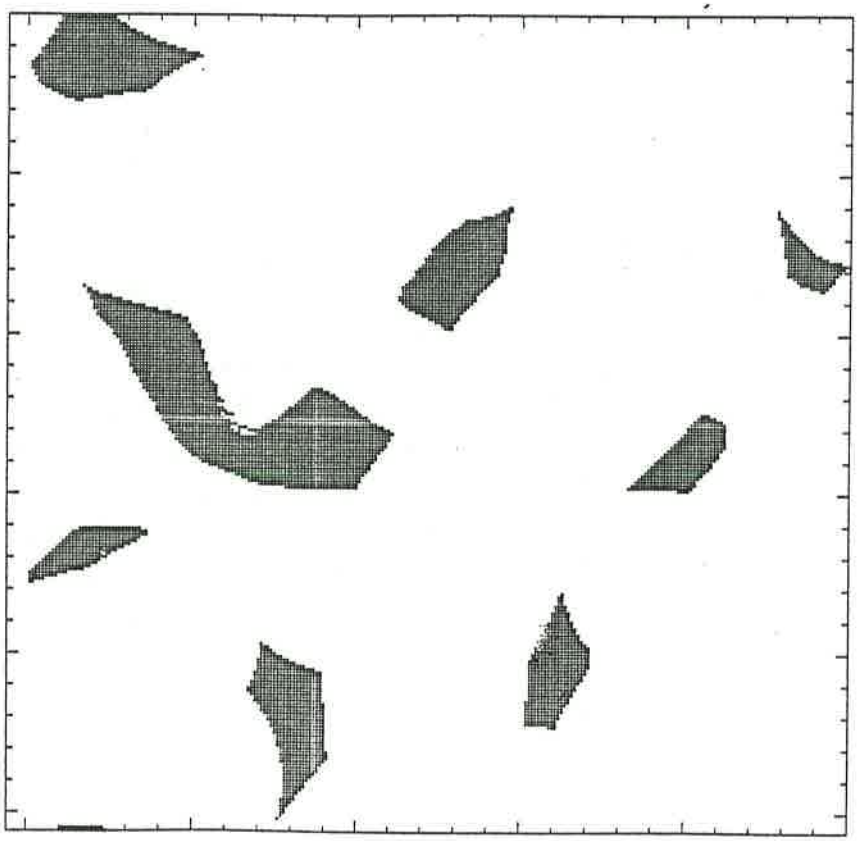

Fig. 11e

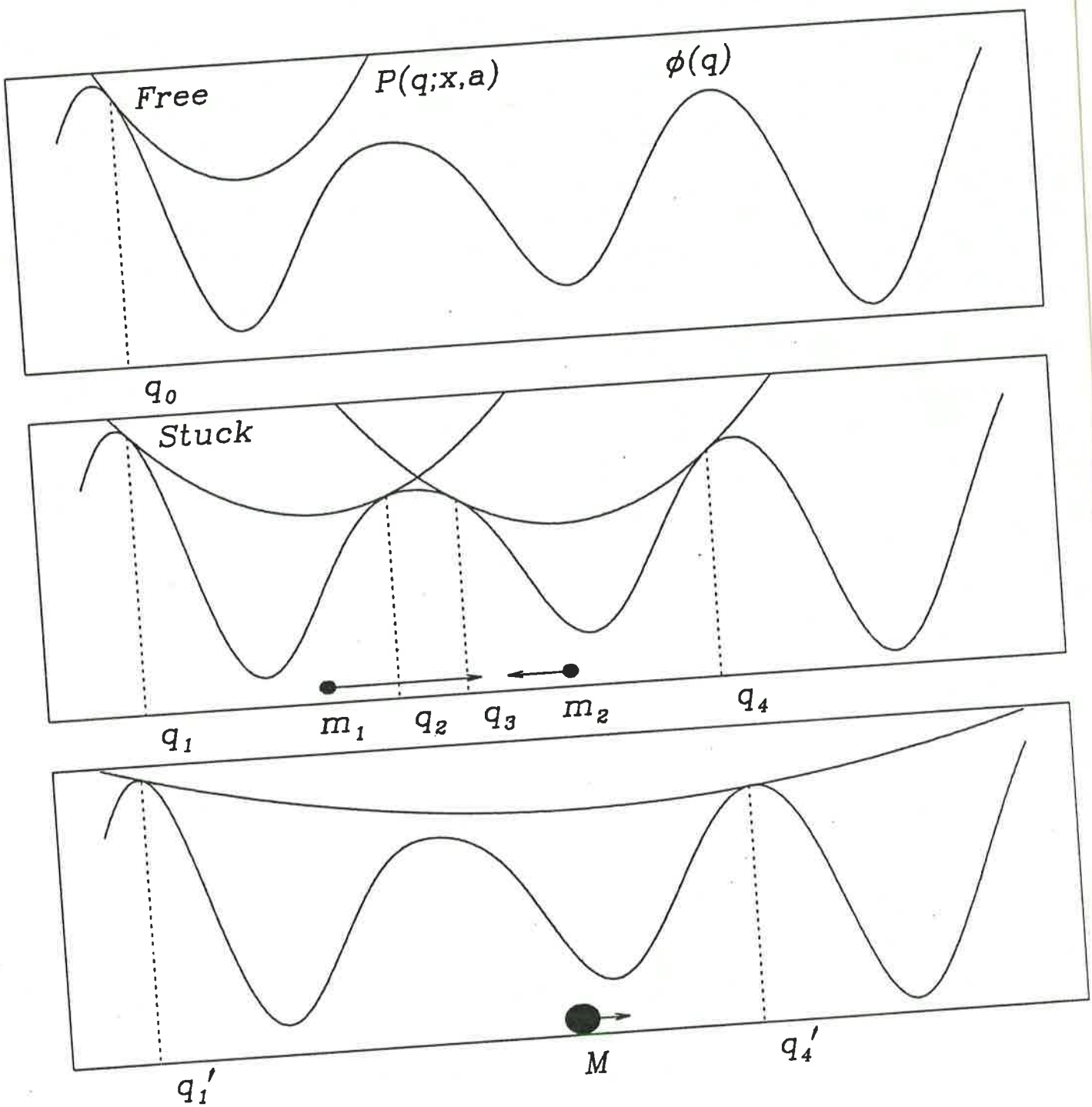


Fig.1

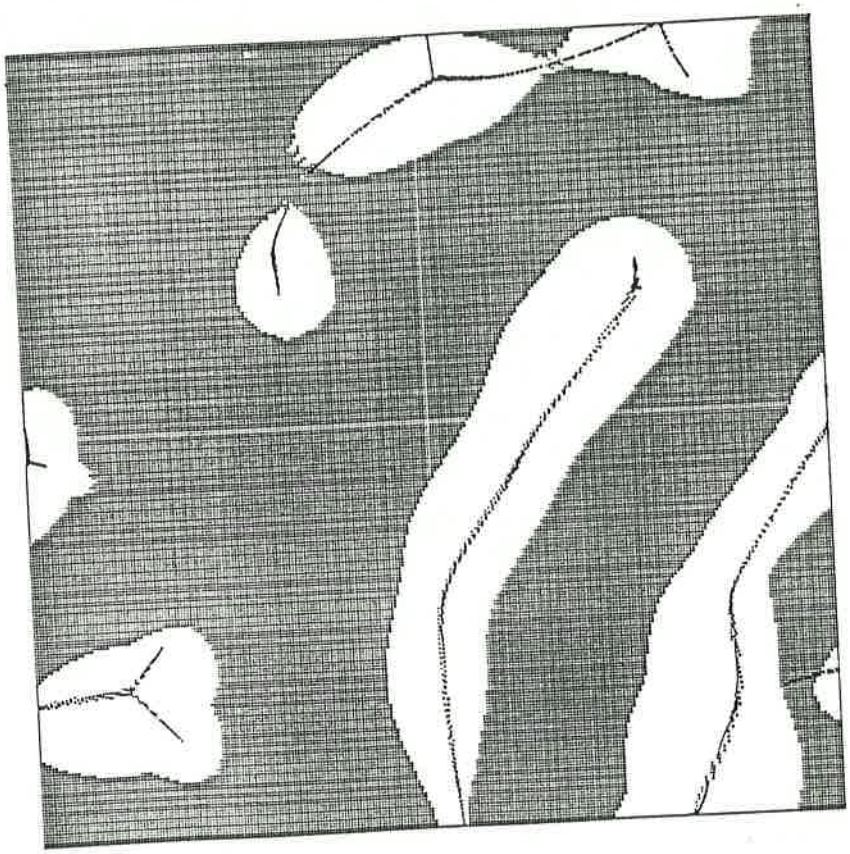

Fig. 2a

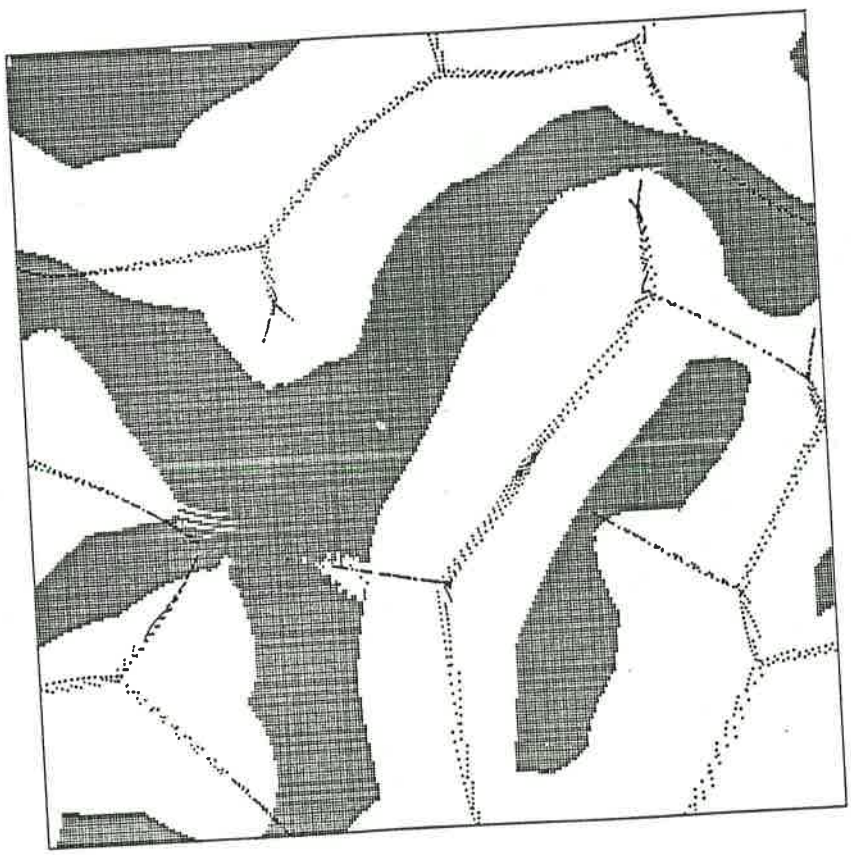

Fig. 2b

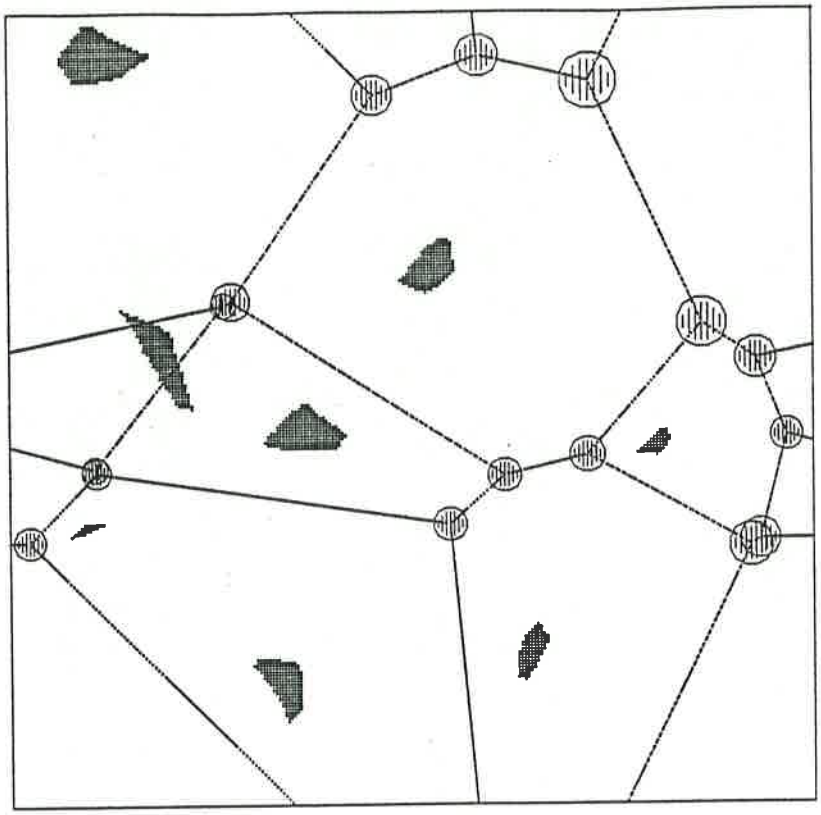

Fig. 2c

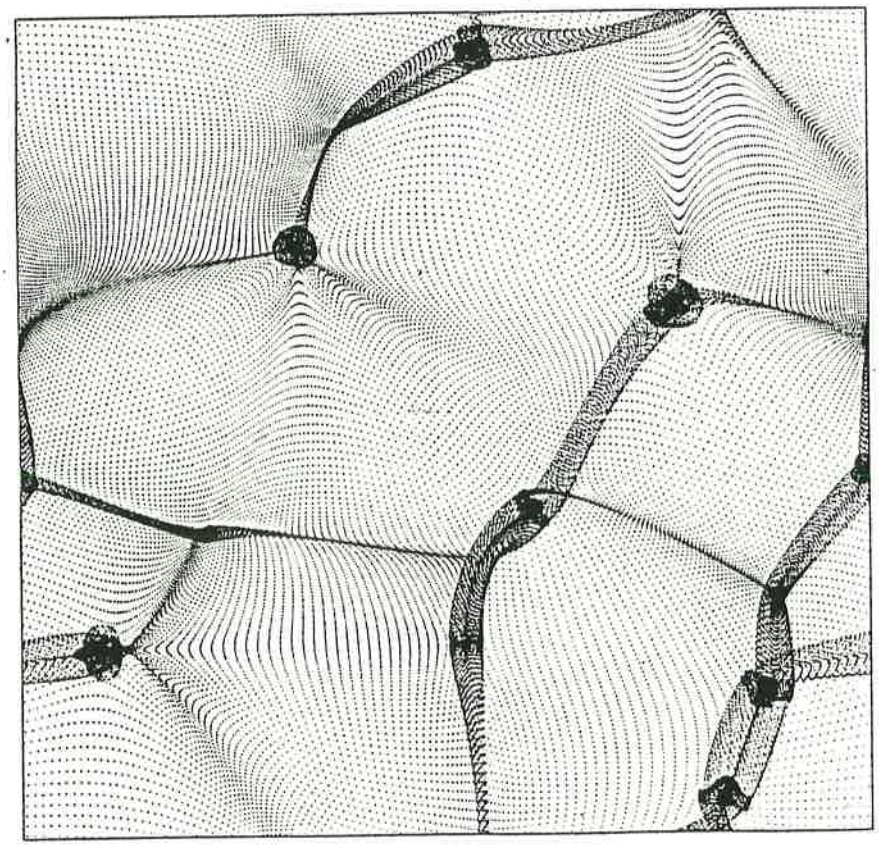

Fig. 2d

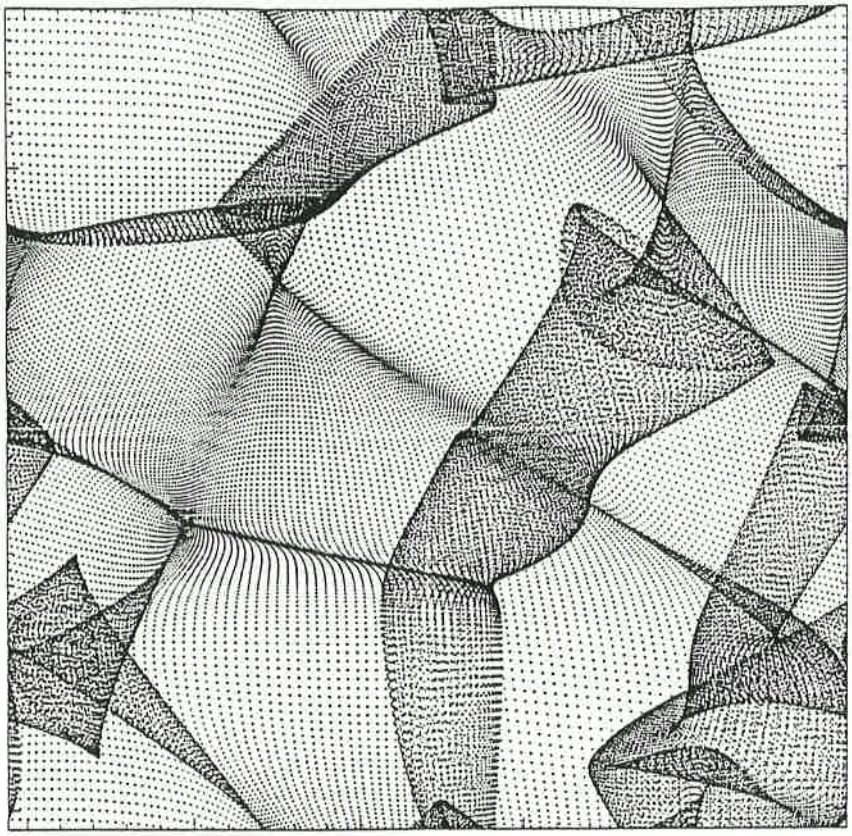

Fig. 2e

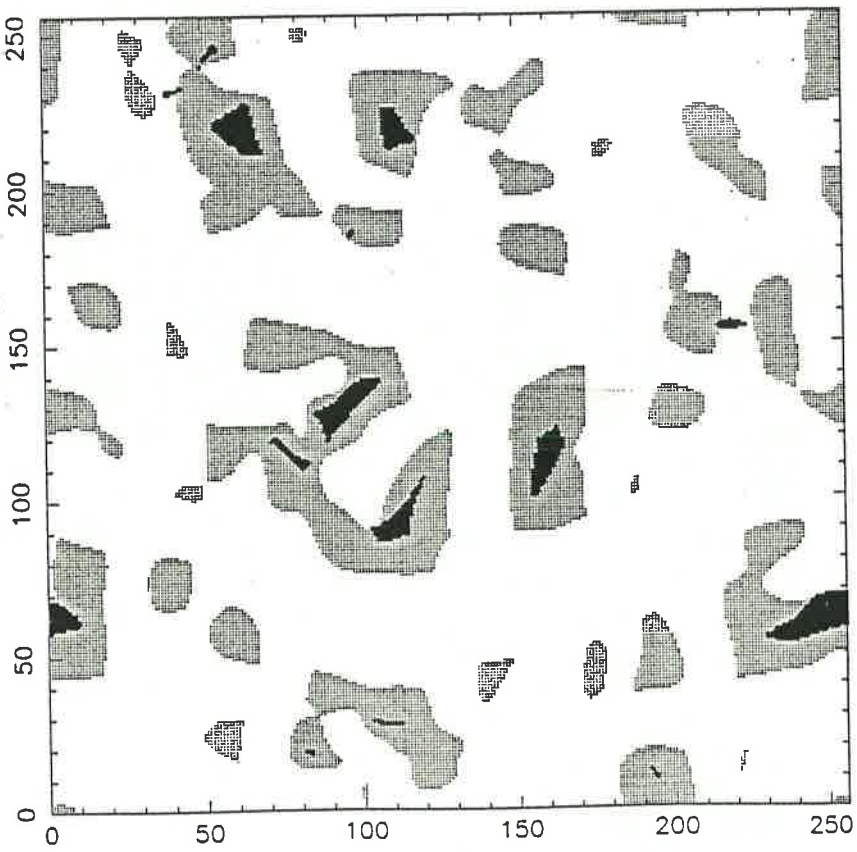


Fig. 3

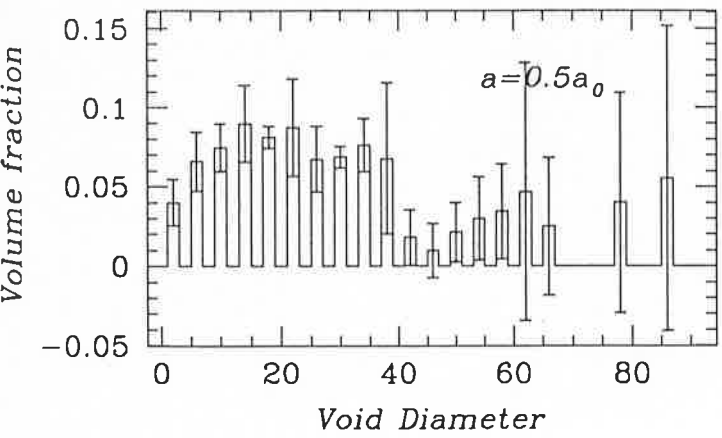
Volume fraction
0.15
0.1
0.05
0
−0.05
a=0.5a0
0
20
40
60
80
Void Diameter

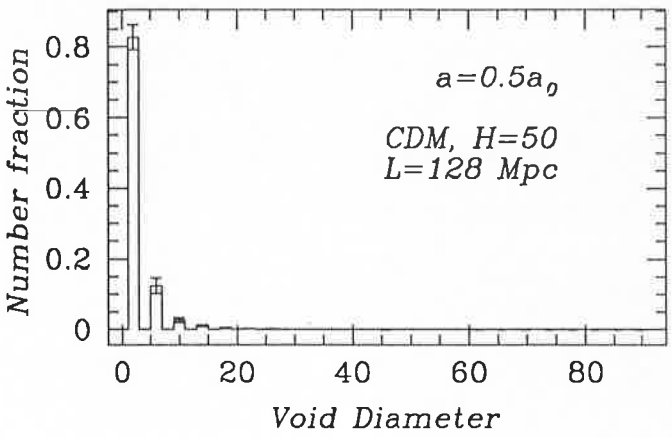
Number fraction
0.8
0.6
0.4
0.2
0
a=0.5a0
CDM, H=50
L=128 Mpc
0
20
40
60
80
Void Diameter

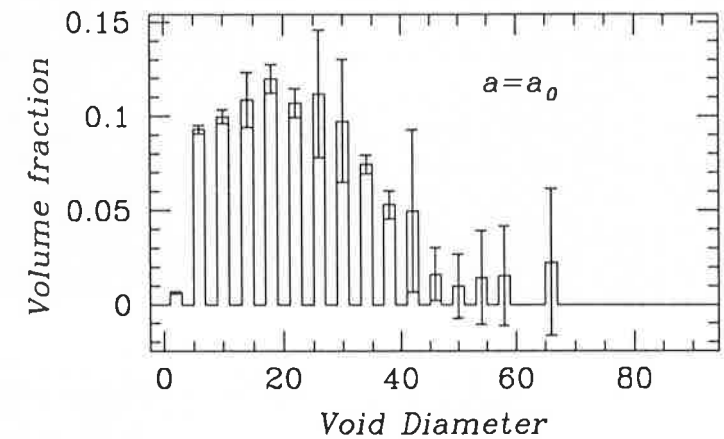
Volume fraction
0.15
0.1
0.05
0
a=a0
0
20
40
60
80
Void Diameter

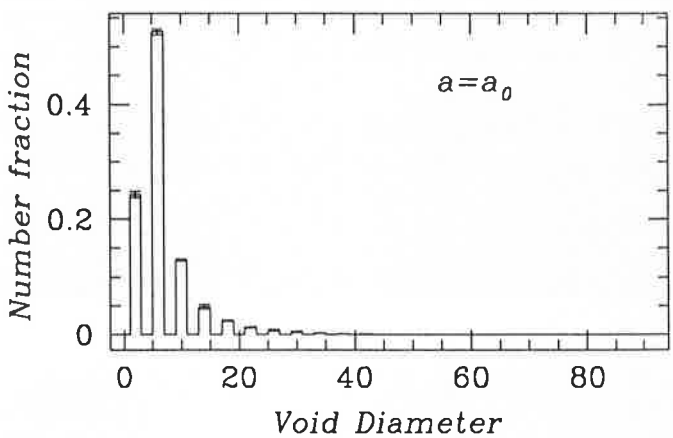
Number fraction
0.4
0.2
0
a=a0
0
20
40
60
80
Void Diameter

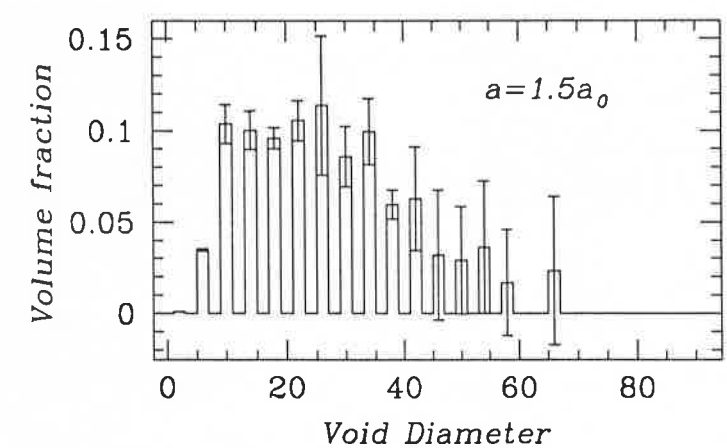
Volume fraction
0.15
0.1
0.05
0
a=1.5a0
0
20
40
60
80
Void Diameter

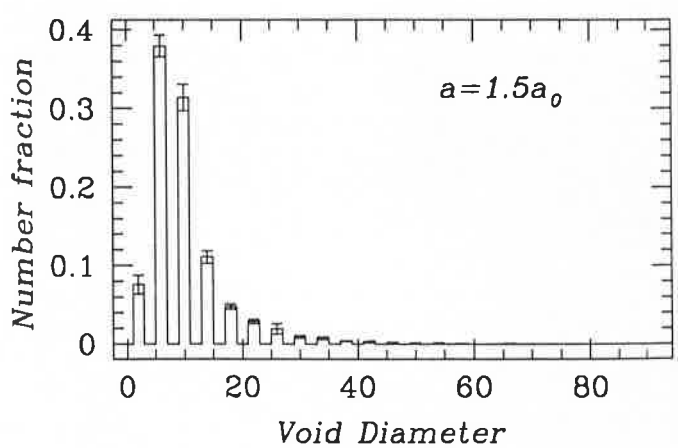
Number fraction
0.4
0.3
0.2
0.1
0
a=1.5a0
0
20
40
60
80
Void Diameter

Fig. 4

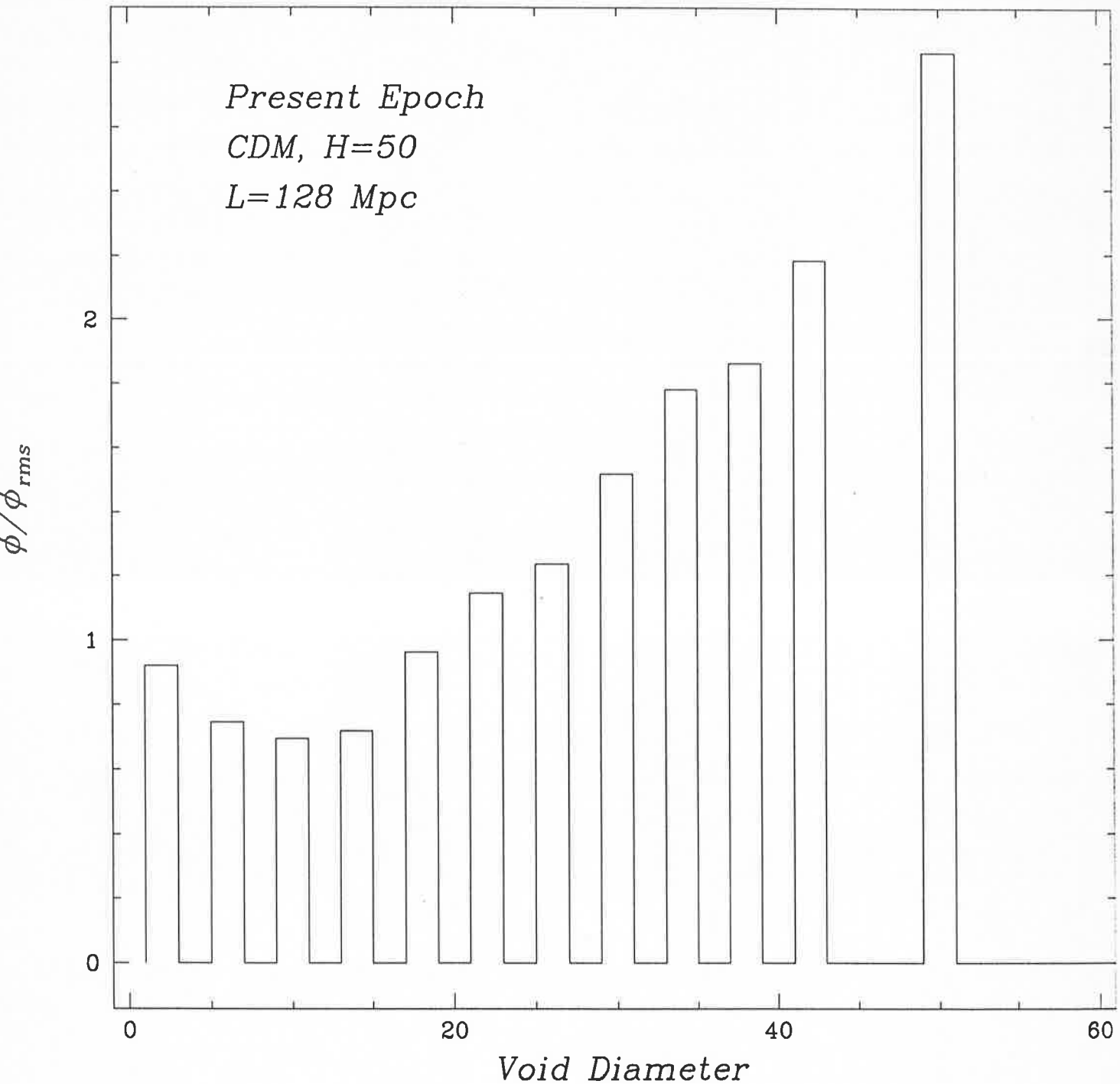
Present Epoch
CDM, H=50
L=128 Mpc
2
1
0
$\phi/\phi_{rms}$
0
20
40
60
Void Diameter

Fig. 5

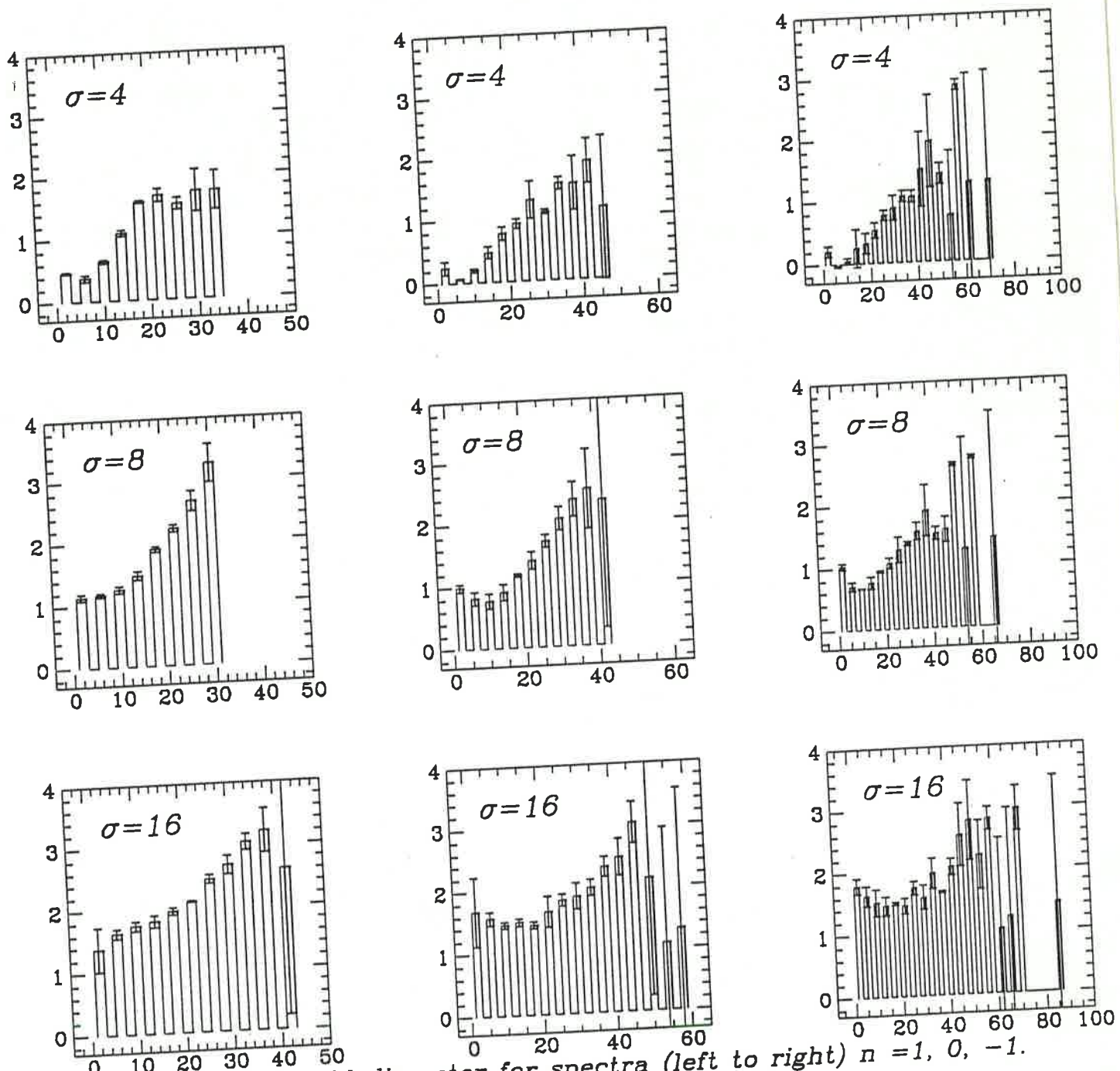


$\phi/\phi_{rms}$ vs. void diameter for spectra (left to right) $n$ =1, 0, −1.

Fig. 6

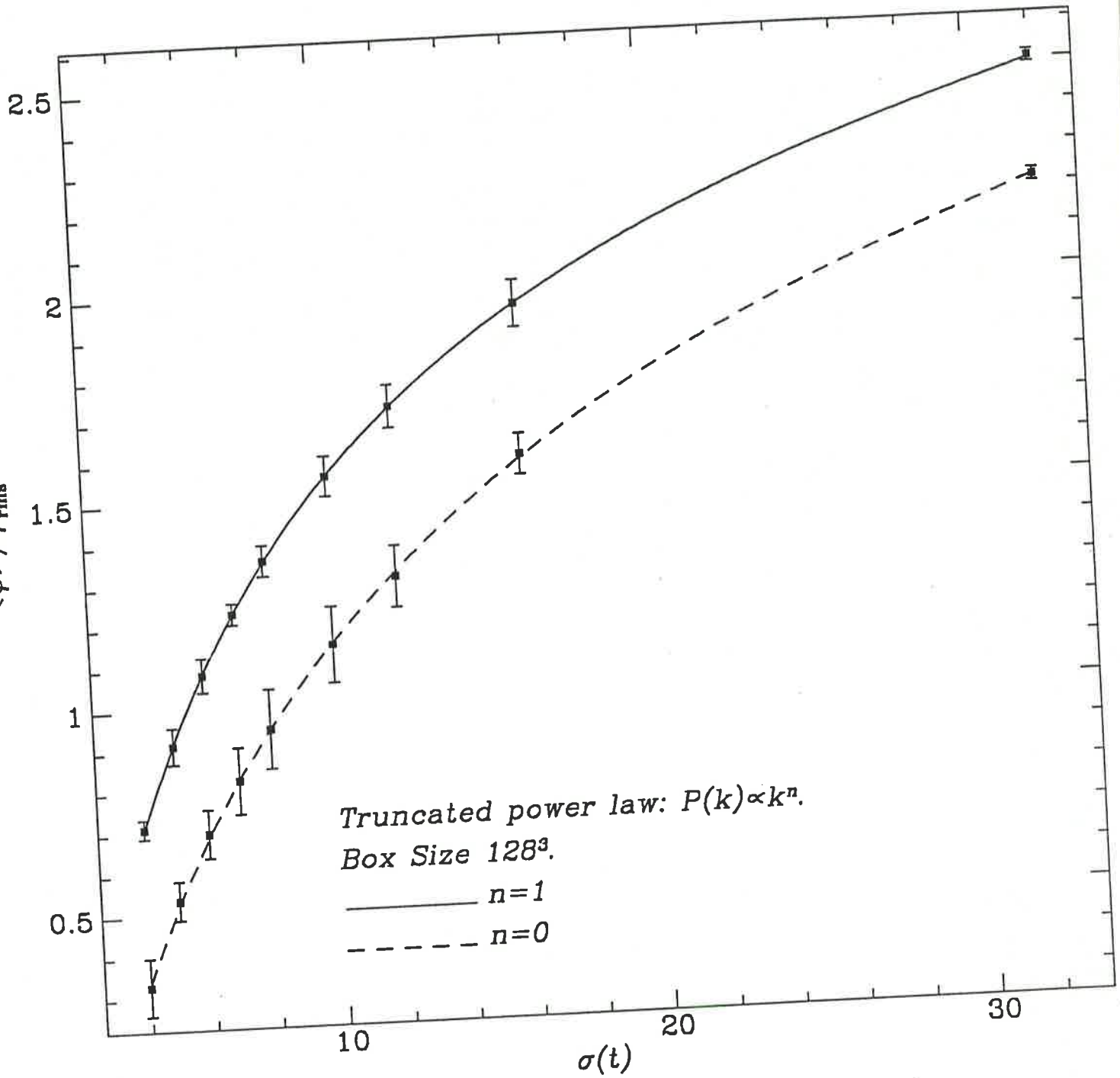
2.5
2
1.5
1
0.5
10
20
30
σ(t)
Truncated power law: P(k)∝k^n.
Box Size 128^3.
n=1
n=0

Fig. 7

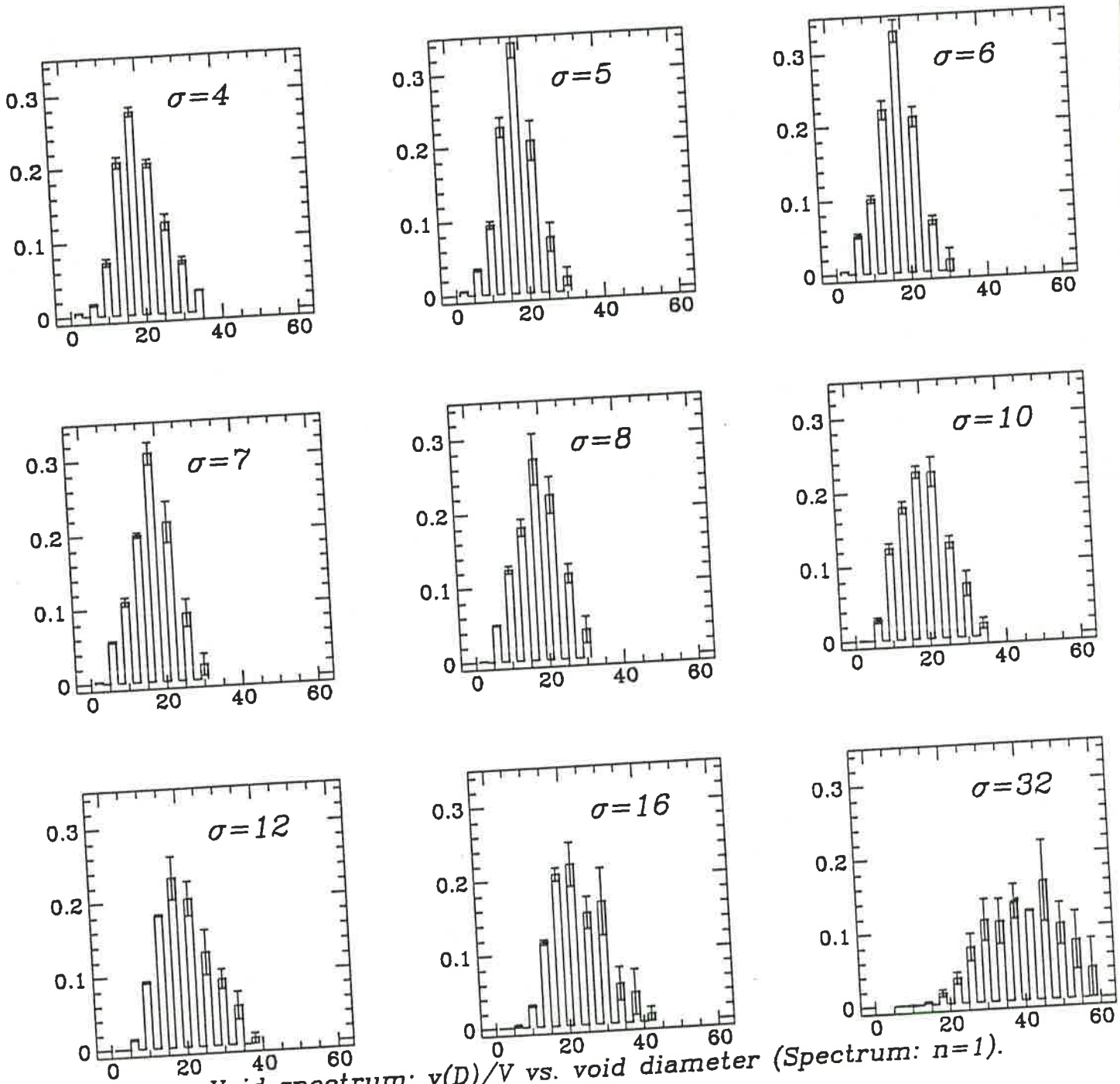


*Void spectrum: v(D)/V vs. void diameter (Spectrum: n=1).*

Fig. 8a

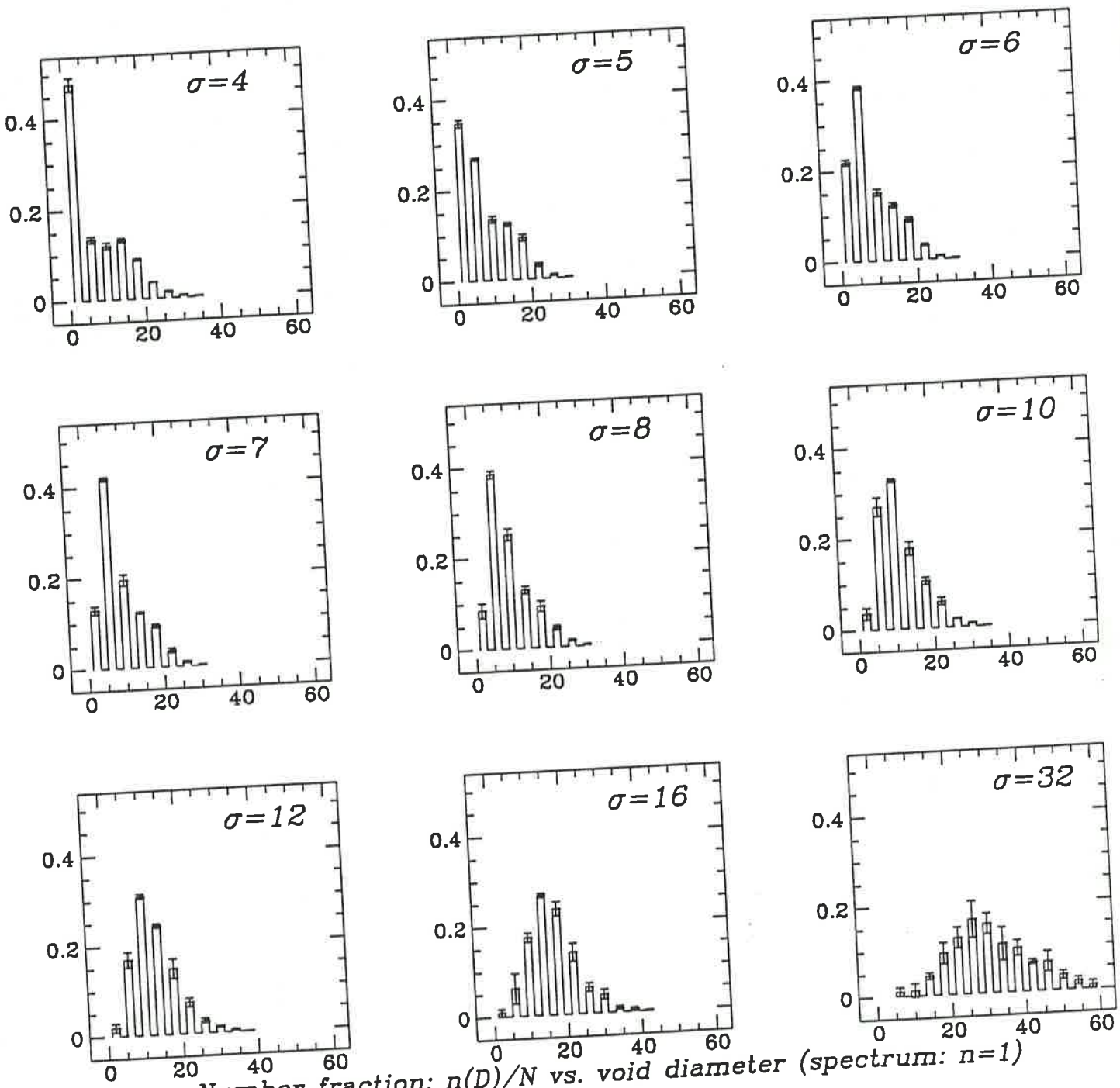


*Number fraction: n(D)/N vs. void diameter (spectrum: n=1)*

Fig. 8b

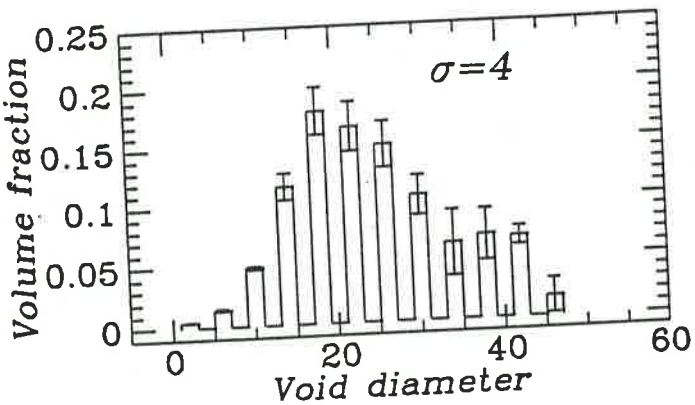
Volume fraction
0.25
0.2
0.15
0.1
0.05
0
σ=4
0
20
40
60
Void diameter

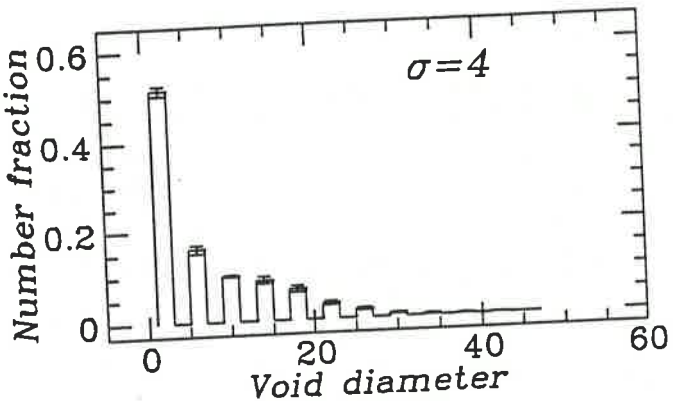
Number fraction
0.6
0.4
0.2
0
σ=4
0
20
40
60
Void diameter

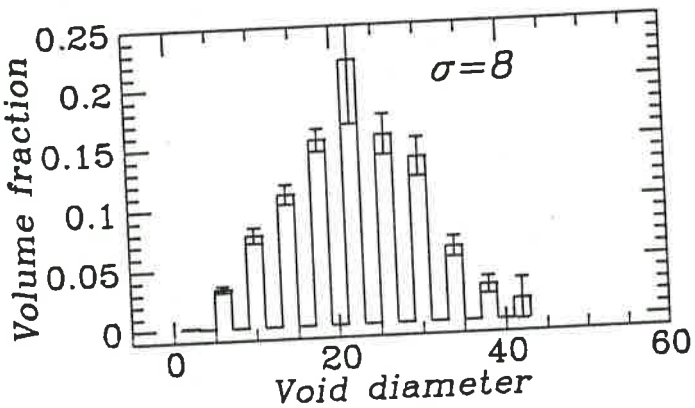
Volume fraction
0.25
0.2
0.15
0.1
0.05
0
σ=8
0
20
40
60
Void diameter

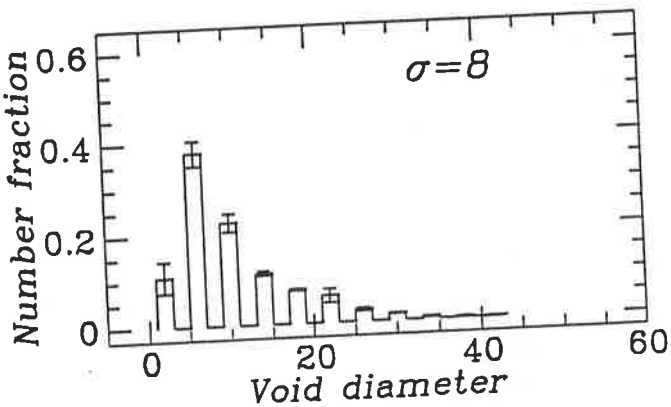
Number fraction
0.6
0.4
0.2
0
σ=8
0
20
40
60
Void diameter

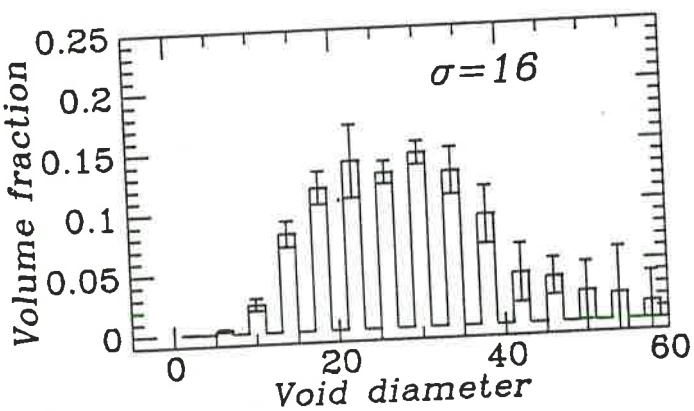
Volume fraction
0.25
0.2
0.15
0.1
0.05
0
σ=16
0
20
40
60
Void diameter

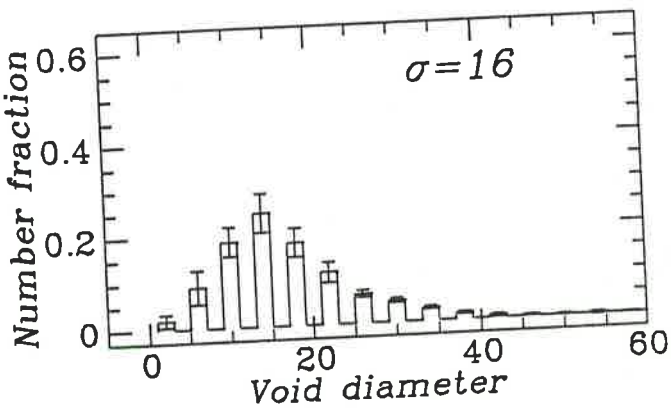
Number fraction
0.6
0.4
0.2
0
σ=16
0
20
40
60
Void diameter

Fig. 8c

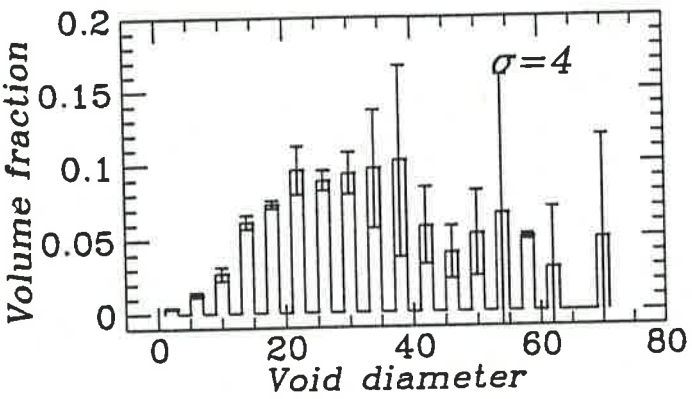
Volume fraction
0.2
0.15
0.1
0.05
0
σ=4
0
20
40
60
80
Void diameter

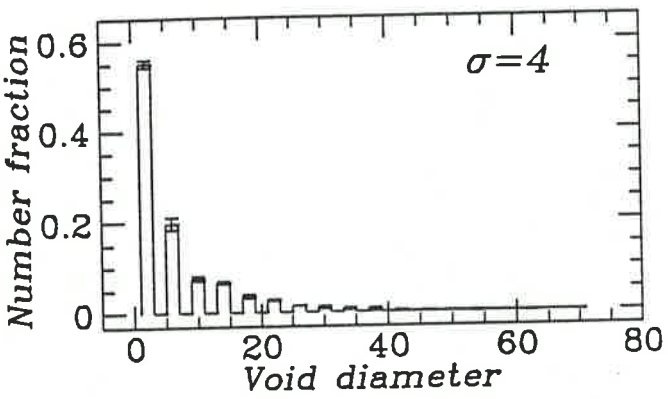
Number fraction
0.6
0.4
0.2
0
σ=4
0
20
40
60
80
Void diameter

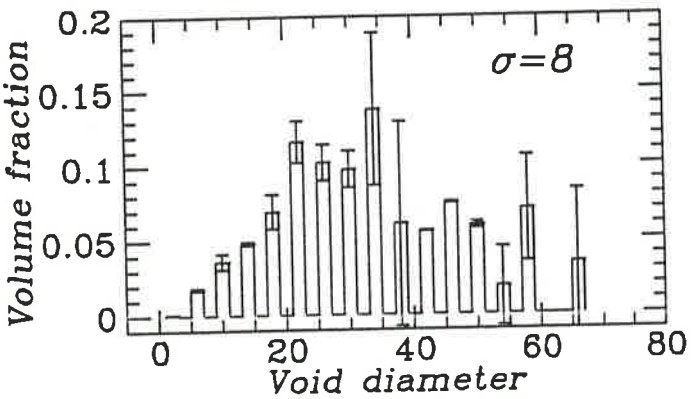
Volume fraction
0.2
0.15
0.1
0.05
0
σ=8
0
20
40
60
80
Void diameter

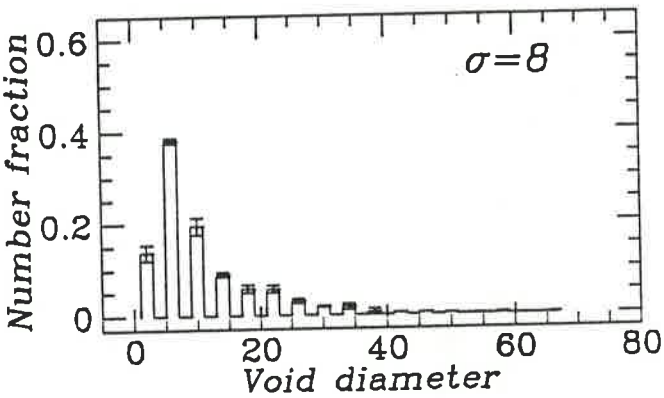
Number fraction
0.6
0.4
0.2
0
σ=8
0
20
40
60
80
Void diameter

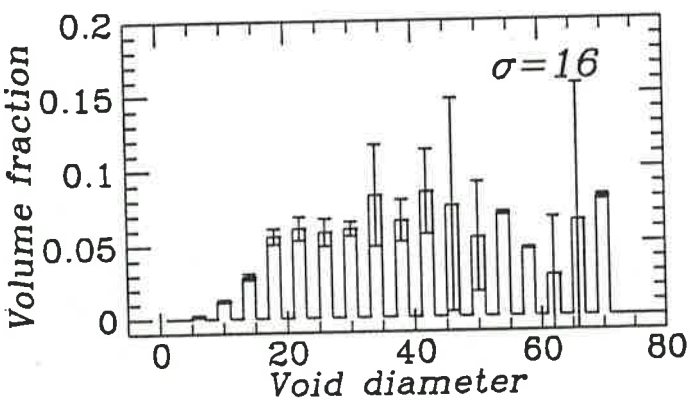
Volume fraction
0.2
0.15
0.1
0.05
0
σ=16
0
20
40
60
80
Void diameter

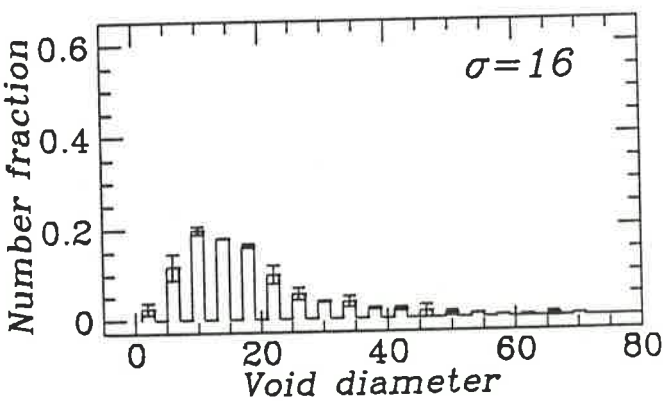
Number fraction
0.6
0.4
0.2
0
σ=16
0
20
40
60
80
Void diameter

Fig. 8d

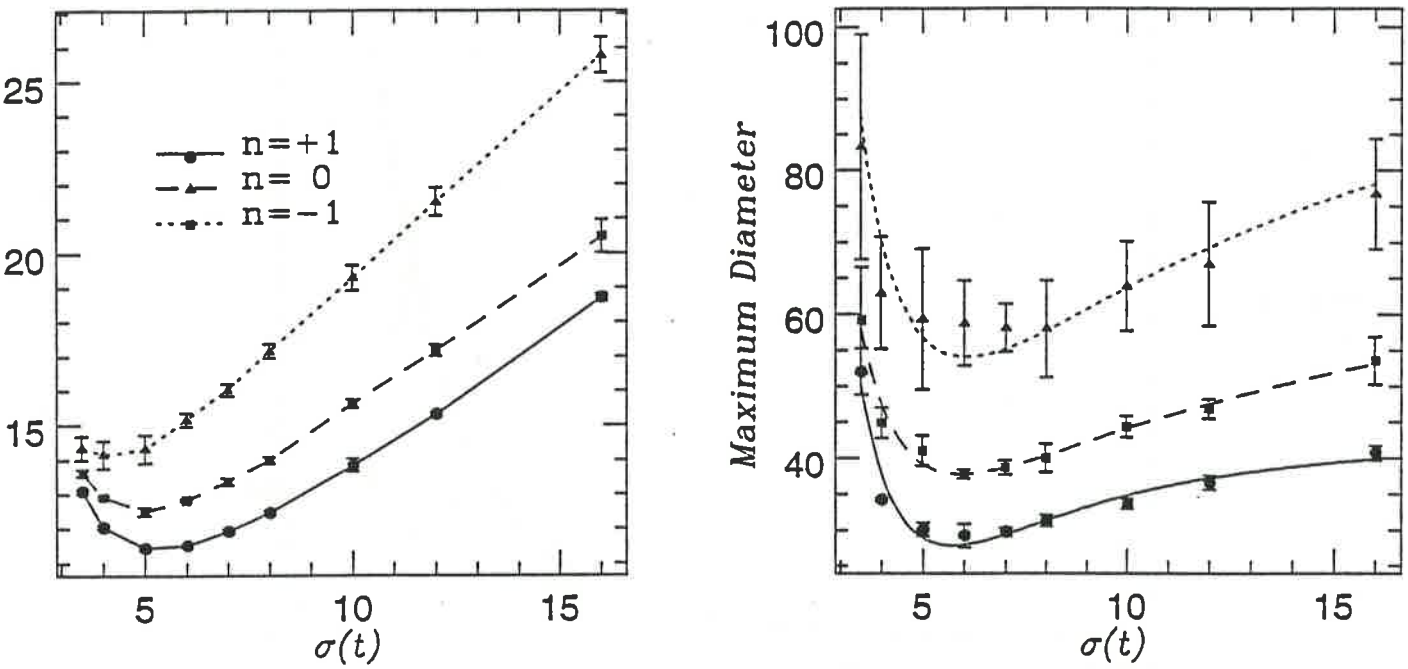
n=+1
n= 0
n=−1
25
20
15
5
10
15
σ(t)
Maximum Diameter
100
80
60
40
5
10
15
σ(t)

Fig. 9a

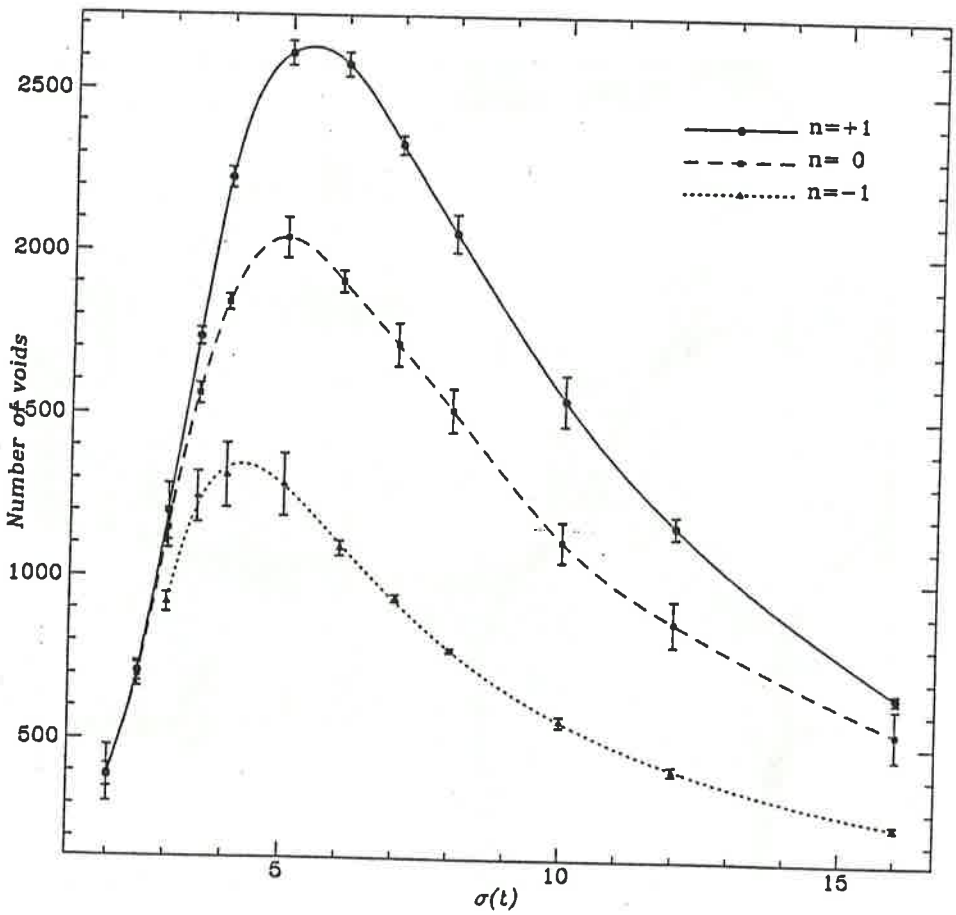
n=+1
n= 0
n=−1
2500
2000
1500
1000
500
Number of voids
5
10
15
σ(t)

Fig. 9b

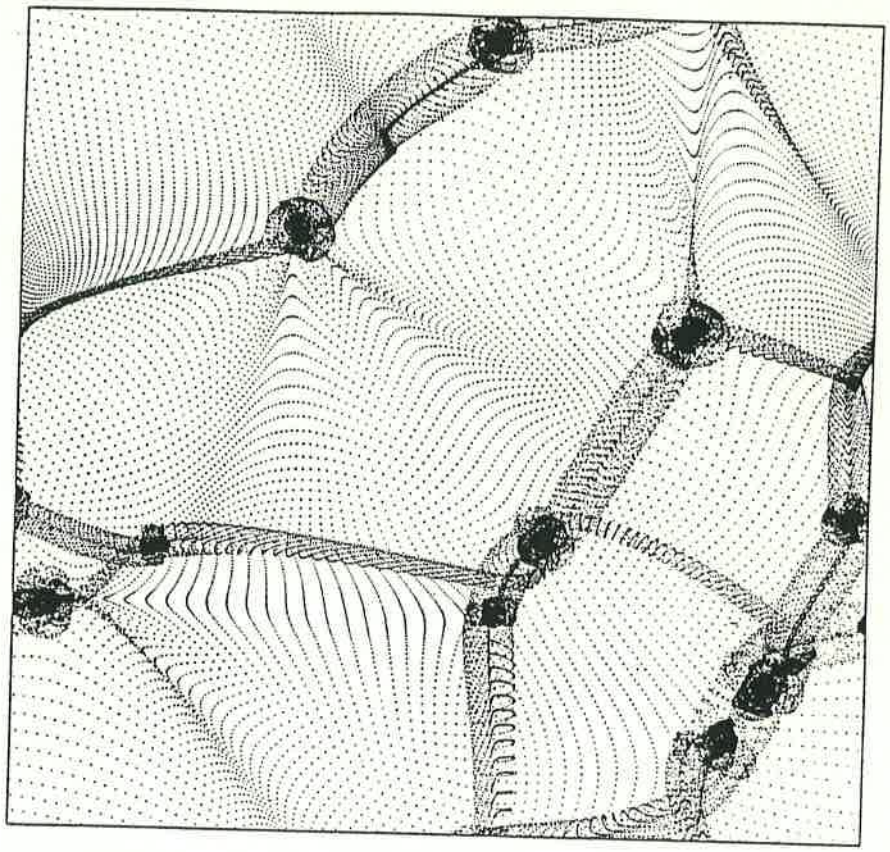

Fig. 11b

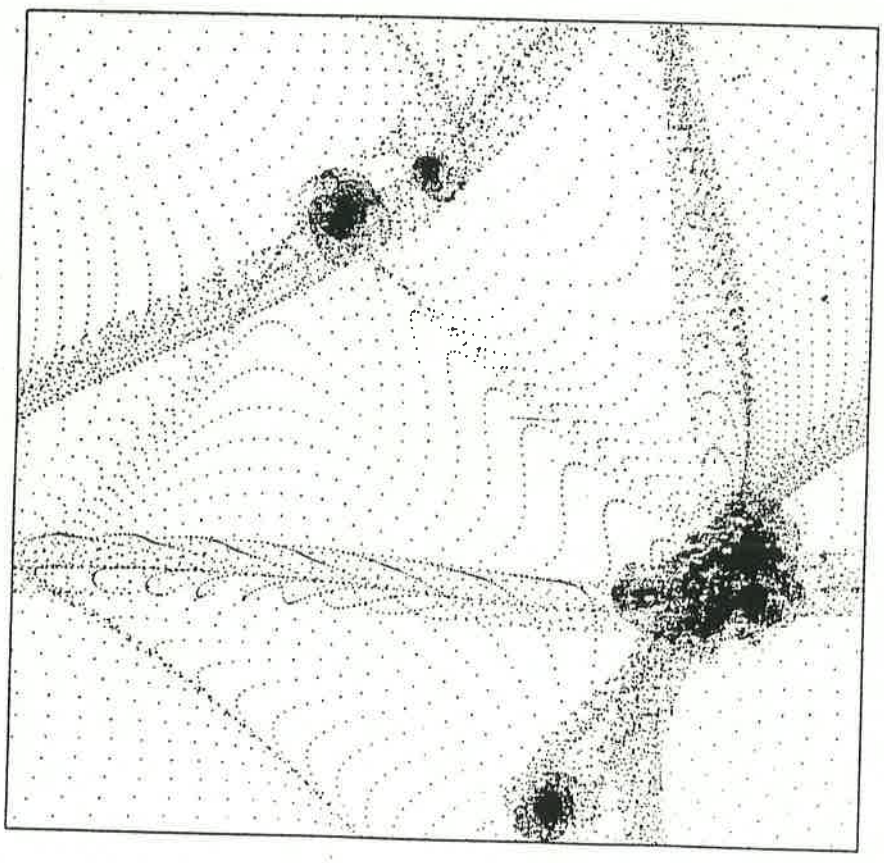

Fig. 11c